Journal of Geochemical Exploration 180 (2017) 71–90

Contents lists available at ScienceDirect

Journal of Geochemical Exploration

journal homepage: www.elsevier.com/locate/gexplo

Bauxite formation on Proterozoic bedrock of Suriname

Dewany A. Monsels[a,b,*], Manfred J. van Bergen[b]

[a] Department of Geology and Mining, Anton de Kom University of Suriname, Leysweg 86, Paramaribo, Suriname
[b] Department of Earth Sciences, Utrecht University, Budapestlaan 4, 3584CD Utrecht, The Netherlands

ARTICLE INFO

Keywords:
Bauxite
Guiana Shield
Tropical weathering
Element mobility
Bauxite textures

ABSTRACT

Lateritic bauxite deposits in Suriname rest on a variety of metamorphic, igneous and sedimentary parent rocks. Remnants of multiple planation surfaces with duricrusts that mark the tropical landscape are associated with recurrent episodes of bauxite formation since Late Cretaceous times. Plateau-type bauxites at the highest topographic levels developed on a range of Proterozoic crystalline bedrocks on the northern edge of the Guiana Shield in the country's interior. Weathering profiles of the Bakhuis Mountains, Nassau Mountains, Lely Mountains and Brownsberg largely correspond to the classical sequence of an iron-rich cap on top of a bauxite layer that covers a clay-rich saprolite interval grading into weathered and fresh bedrock. All of the investigated profiles are consistent with in-situ formation of the bauxite and are marked by Si-Al-Fe relationships indicative of medium to strong lateritization, with fresh bedrock being poorly exposed. The bauxite deposits contain gibbsite as the dominant Al-bearing phase, whereas boehmite is locally present in subordinate quantities. Their ferruginous character is expressed by relatively abundant goethite and hematite in the top layers. Kaolinite is the main mineral in the saprolite. Anatase and zircon are the most detected minor phases. The investigated bauxite deposits are generally of a medium-grade (average Al_2O_3 contents 33–49 wt%) but have variable chemical compositions according to exploration drilling results. Average Fe_2O_3 contents (13–34 wt%) show inverse relationships with Al_2O_3. Despite this overall conformity of the deposits, their thicknesses, textures, mineralogy and geochemistry are distinct in detail, reflecting contrasts in the nature of the parent rock and weathering history. Inter-element relationships show conspicuous differences between SiO_2-poor (< 5 wt%) upper parts and SiO_2-richer (> 5 wt%) lower parts of profiles in the Bakhuis Mountains, which developed on high-grade metamorphic pyroxene amphibolites and gneissic granulites. The bauxites of the Nassau Mountains and the other areas in eastern Suriname are marked by higher TiO_2 contents (average > 3.9 wt%) and dissimilar profiles that reflect their development on variety of a low-grade metamorphic volcanic parent rocks. Weathering-induced redistribution of rare-earth and other trace elements affected even the least mobile elements. Differences in distribution patterns between individual profiles can be attributed to a combination of primary compositional differences of parent rocks, the nature and content of accessory mineral phases, and unequal responses to multiple bauxitization cycles.

1. Introduction

Lateritic bauxites of economic interest have formed on a range of different sedimentary, igneous and metamorphic parent rocks worldwide. A sufficiently high aluminium content, together with favorable physical rock properties and weathering conditions determines the potential of a bauxite deposit as raw material for the aluminium industry (Valeton, 1972; Schellmann, 1983; Bárdossy and Aleva, 1990; Patterson et al., 1986; Aleva, 1994; Tardy, 1997). Widespread lateritic bauxite deposits on the Amazonian Craton and bordering coastal regions of South America formed by extensive weathering in Late Cretaceous–Early Tertiary times (Bárdossy and Aleva, 1990). Because a warm and humid climate is a critical requirement for their origin, the weathering profiles of these South-American bauxites show similarities with equivalent regolith profiles in other low-latitude (paleo-) tropical or (paleo-) equatorial regions in Africa, South Asia and Australia (Bárdossy and Aleva, 1990; Bogatyrev et al., 2009; Tardy and Roquin, 1998; Horbe and Anand, 2011; Mutakyahwa and Valeton, 1995, and references therein). All these deposits are distributed on tectonically stable post-Gondwanan continental landmasses.

In Suriname, bauxite developed on a variety of parent rocks ranging from Tertiary sedimentary rocks to Precambrian igneous and metamorphic basement lithologies. Mining activities commenced about a century ago (Aleva and Wong, 1998) and have been restricted to

* Corresponding author at: Department of Geology and Mining, Anton de Kom University of Suriname, Leysweg 86, Paramaribo, Suriname.
E-mail addresses: dewany.monsels@uvs.edu (D.A. Monsels), m.j.vanbergen@uu.nl (M.J. van Bergen).

http://dx.doi.org/10.1016/j.gexplo.2017.06.011
Received 25 October 2016; Received in revised form 24 May 2017; Accepted 17 June 2017
Available online 20 June 2017
0375-6742/

deposits in the coastal plain where bauxite formed mostly on arkosic or silty sedimentary parent rock (Aleva, 1965, 1979). Together with a refinery industry, the exploitation of these bauxite resources made Suriname one of the World's leading exporters of bauxite and alumina around the 1950s (Bárdossy and Aleva, 1990; Patterson et al., 1986; Monsels, 2016). In contrast, bauxites on plateaus in Suriname's interior, which originated on Proterozoic crystalline parent rocks of the Guiana Shield, have not been productive so far, although they have been comprehensively explored for their economic potential (e.g., Doeve, 1955; Van Kersen, 1956; Krook and De Roever, 1975; Pollack, 1981, 1983; Aleva and Hilversum, 1984).

Studies targeting vertical distributions of major and trace elements together with mineralogy in weathering profiles of bauxite deposits developed on Precambrian igneous rocks of the Amazonian Craton are scarce. Recent examples concern the Los Pijiguaos bauxite deposit, Venezuela, which developed on granite (Meyer et al., 2002), and deposits on granitic and volcanic bedrocks in Brazilian Amazonia (Horbe and Anand, 2011). Similar work on Suriname's plateau bauxites is limited to an early study of Topp et al. (1984). The objective of this paper is to provide new insights into the weathering processes that created the plateau-type or plateau bauxites in Suriname's interior from a variety of Precambrian crystalline bedrocks. Vertical mineralogical, textural and geochemical variations in weathering profiles are presented to discuss critical processes in the origin of the bauxite duricrusts and to assess the effect of parent-rock properties.

Throughout the paper we will use “laterite” loosely as a geologic term for a rock that experienced intense subaerial weathering, consists predominantly of goethite, hematite, aluminium hydroxides, kaolinite and quartz, and has a $SiO_2/(Al_2O_3 + Fe_2O_3)$ ratio lower than that of the associated kaolinized parent rock. “Bauxite” will be used for a laterite enriched in free aluminium hydroxide minerals such as gibbsite and boehmite (cf., Bárdossy and Aleva, 1990).

2. Geological setting

2.1. Bauxites in Suriname

Suriname is part of the Guiana Shield in the north-eastern section of South America. Proterozoic rocks make up about 80% of the country (Crystalline Basement) and the remaining 20% consists of Cretaceous to Recent sediments that were deposited along the northern fringe of the craton (Coastal Area) (Fig. 1a). The Proterozoic basement of Suriname consists of three metamorphic belts: the low-grade Marowijne Greenstone belt in the NE and the high-grade Bakhuis Granulite belt and the Coeroeni Gneiss Belt in the NW and SW, respectively (Kroonenberg et al., 2016). These belts are separated by a large area consisting of various types of granitoid rocks and felsic volcanic rocks in the central part of the country. The basement is overlain by a remnant of the Proterozoic Roraima Formation in the Tafelberg sandstone plateau, and transected by Proterozoic and Early Jurassic dolerite dykes (Fig. 1a).

Surinamese bauxite deposits have formed on two different types of parent rock (Fig. 1a; see also Monsels, 2016 and references therein):

1. Crystalline rocks in the hinterland (Plateau or Highland bauxites). As part of the Guiana Shield subprovince (Van Kersen, 1956; Janssen, 1979; Bárdossy and Aleva, 1990), these bauxites are mostly developed on intermediate to mafic Precambrian crystalline igneous or metamorphic rocks.
2. Sedimentary rocks in the coastal area (Coastal-plain or Lowland bauxites). These bauxites belong to the Coastal-plain subprovince and the so-called “Bauxite belt”, which continues into Guyana and runs subparallel to the “Old coastal plain’, an accumulation of continental sediments that were deposited along a paleo-coastline in Early Cenozoic times (Van der Hammen and Wijmstra, 1964; Valeton, 1983; Aleva and Wong, 1998; Wong et al., 1998).

Both groups of deposits are part of a sequence of five bauxitic or Fe-lateritic surface levels that have been distinguished in Suriname and neighbouring territories (King et al., 1964; Pollack, 1983; Aleva, 1984; Bárdossy and Aleva, 1990; Tardy and Roquin, 1998; cf. Fig. 1b). The succession of planation surfaces developed in different episodes between Late Cretaceous and Quaternary times, with the Early Teriary as most prominent interval of bauxite formation. The bauxite deposits studied here are typical plateau bauxites of the Bakhuis Mountains, Nassau Mountains, Lely Mountains and Brownsberg (Fig. 1a), which formed on a variety of metamorphosed crystalline parent rocks in this part of the Precambrian Guiana Shield, including (ultra)mafic to intermediate metavolcanics and greenschists.

2.2. Local geology of plateau bauxites

2.2.1. Bakhuis Mountains bauxite district

The *Bakhuis Mountains* (04°00′–05°00′N, 56°30′–57°30′W), which form a chain of strongly dissected plateaus, are an expression of a 25 km wide and 95 km long NE-SW striking horst, one of the many structural features of the Bakhuis-Kanuku zone in the heart of the Guiana Shield (Kroonenberg and De Roever, 1975; Kroonenberg, 1976; Kroonenberg and Melitz, 1983; Kroonenberg et al., 2016). Hilltops reach heights of approximately + 480 m a.s.l. The climate is tropical humid with an average temperature of 27.5 °C and 1700–2200 mm of rainfall, divided over a long and a short rainy season. The basement of the Bakhuis Mountains consists of the high-grade metamorphic Falawatra Group, which includes banded rocks from a charnockite suite, sillimanite gneisses and clinopyroxene amphibolites (Figs. 1a, 2a) (De Roever et al., 1976, 2003; Klaver et al., 2015; Kroonenberg et al., 2016). Zircon ages of the charnockites range from 1984.4 to 1992.5 Ma, while a zircon from a leucosome, formed under UHT conditions, revealed an age of 2172.6 ± 7.3 Ma (Klaver et al., 2015).

Variable compositions of bauxite weathering profiles reflect the large diversity of parent rocks (Aleva and Hilversum, 1984), which, together with differences in drainage conditions is also responsible for variability in thickness of the bauxite body. Locally, lenses of kaolinite-rich material occur within the bauxite horizon, and lenses and boulders of bauxite material within the kaolinitic saprolite (Pollack, 1981; Aleva and Hilversum, 1984). Exposures of fresh bedrock and boulders along slopes, hill tops, creek beds and within the lateritic bauxite body are common. Different topographic levels of the Bakhuis duricrusts suggest two distinct events of bauxite formation. Bárdossy and Aleva (1990) attributed an Eocene age to the top surface (which includes the investigated Area 10 profiles) and a Miocene age to the lower surface, while Pollack (1983) assigned a Late Cretaceous and Eocene age, respectively. A paleomagnetic age of 60 ± 20 Ma (Théveniaut and Freyssinet, 2002) is grossly consistent with the interpretation of Pollack (1983) and an earlier proposed age of 70 Ma (Billiton, 1979). The bauxite resources of the Bakhuis Mountain are estimated to be larger than 500 Mt. and contain an average of 34% available alumina and 2% reactive silica (Bauxite Institute Suriname, 2009).

2.2.2. Nassau Mountains bauxite district

The Nassau bauxite district in eastern Suriname includes the bauxite- laterite-covered high plateaus of the Nassau Mountains, Lely Mountains, and Brownsberg (Bárdossy and Aleva, 1990, and references therein), distributed around the Van Blommenstein Lake (Figs. 1a, 2b–c). The mountains belong to the NW-SE striking Marowijne Greenstone Belt for which zircon ages between 2.26 and 2.10 Ga have been reported (Delor et al., 2003; Kroonenberg et al., 2016) (Fig. 1a). The belt predominantly consists of low-grade metamorphic mafic to intermediate volcanics, sedimentary rocks and granitoids (Priem et al., 1971, 1980; Bosma et al., 1984; De Vletter, 1984; De Vletter et al., 1998; Kroonenberg et al., 2016). All of the bauxite-capped mountains of this group are made up of rocks from the Paramaka Formation, which mainly consists of greenschist-facies metabasalts but also contains

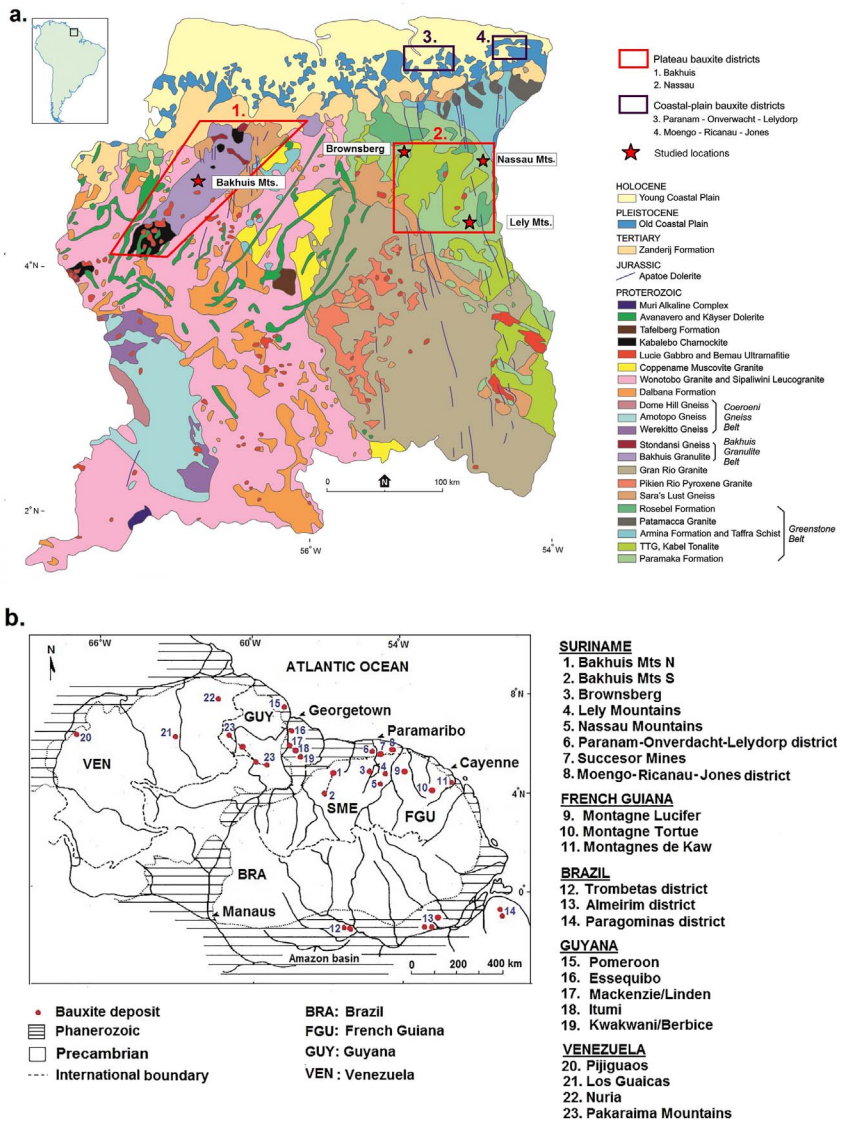

Fig. 1. (a) Geological map of Suriname (after Kroonenberg et al., 2016) and bauxite districts. Areas 1 and 2 represent groups of plateau bauxites, which originated on various metamorphosed crystalline rocks of Precambrian age; those studied here are indicated. Areas 3 and 4 represent groups of coastal-plain bauxite deposits, formed on Early Cenozoic sedimentary parent rocks; most of them are former mining areas; (b) locations and types of bauxite deposits of the Guiana Shield (modified after Bárdossy and Aleva, 1990).

meta-gabbros, meta-andesites, meta-cherts and other intermediate and felsic meta-volcanic rocks (Fig. 1a) (Janssen, 1977; De Vletter, 1984; De Vletter et al., 1998; Bárdossy and Aleva, 1990; Kroonenberg and Melitz, 1983; Kroonenberg et al., 2016). The plateaus have all been tentatively associated to a Late Cretaceous or early Tertiary planation surface (King et al., 1964).

The *Nassau Mountains* (04°46′–04°56′N, 54°30′–54°38′W) form an isolated, U-shaped mountain ridge (20 × 20 km^2), which is bordered by the Van Blommenstein Lake to the west and the Marowijne River to the east (Figs.1b, 2b, c). The ridge comprises four steep-sided, laterite-capped plateaus (A–D) at elevations between 500 and 564 m a.s.l. (Bárdossy and Aleva, 1990; Ter Steege et al., 2006; Bánki et al., 2008). The mountains receive some of the highest rainfall in the country (2750–3000 mm/year, even more on the plateaus). The ridge is covered with high dry-land forest and small areas of wet palm-swamp forest in depressions on the plateaus, and with "mountain savanna" on the northeastern edge of the plateau (Ter Steege et al., 2006; Bánki et al., 2008). A swamp forms in local depressions on Plateau C when rainfall exceeds the infiltration capacity of the local unsaturated zone during wet seasons (Doeve, 1955). A shallow, unconfined aquifer system covers an area of 6.5 km^2 in the porous bauxite (Ouboter et al., 2007).

A Late Cretaceous to Early Tertiary age was assigned to the Nassau bauxite deposit by Bárdossy and Aleva (1990), whereas Aleva and Wong (1998) favored an Eocene-Oligocene age. Doeve (1955) and Van Kersen (1956) characterized the deposit as a multicolored, up to 10 m thick bauxite with variable hardness, showing aphanitic, ooïdal, pisoidal, gravelly and breccia-like textures. The bauxite beds are covered by a dark, up to 5 m thick Fe-rich duricrust, and they are underlain by an up to 15 m thick saprolite composed of soft clayey material. The contact with the saprolite is gradational or sharp, whereas bauxite may also be absent so that locally the duricrust directly overlies the saprolite (Doeve, 1955; Bárdossy and Aleva, 1990). It has been estimated that the Nassau deposit contains between 32 and 60 million dry tonnes of bauxite (Bauxite Institute Suriname, 2009). The most promising areas for mining are Plateaus A and C (Fig. 2b, c).

The *Brownsberg* or *Browns Mountain* (04°46′–05°00′N, 55°08′–55°15′W), situated on the western border of the Van Blommenstein Lake (Fig. 2b), is approximately 34 km long and has a

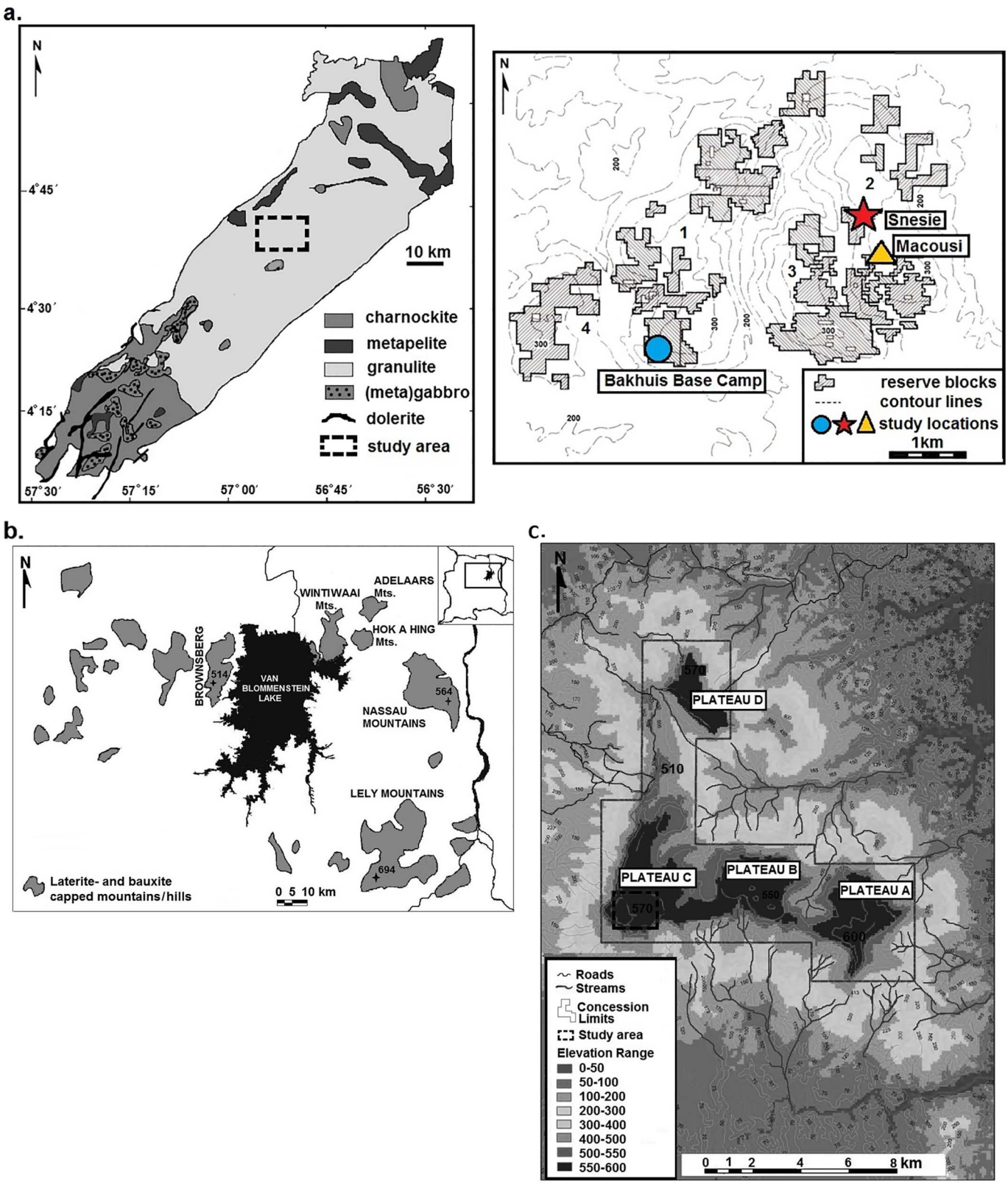

Fig. 2. (a) Geological map of the Bakhuis Mountains horst (modified after Klaver et al., 2015). The study locations Bakhuis Base Camp (exploration Area 10.1) and Snesie and Macousi (Area 10.2) are indicated on the right panel, which represents a magnification of the hyphened rectangle on the left map; (b) laterite- and bauxite capped mountains and hills in NE Suriname (Nassau bauxite district) (modified after Van Lissa, 1975; SPS and OAS, 1988); Ter Steege et al., 2006); (c) elevation map of the Nassau Mountains (modified after Van den Bergh, 2011). Black hyphened rectangle indicates the study area on plateau C.

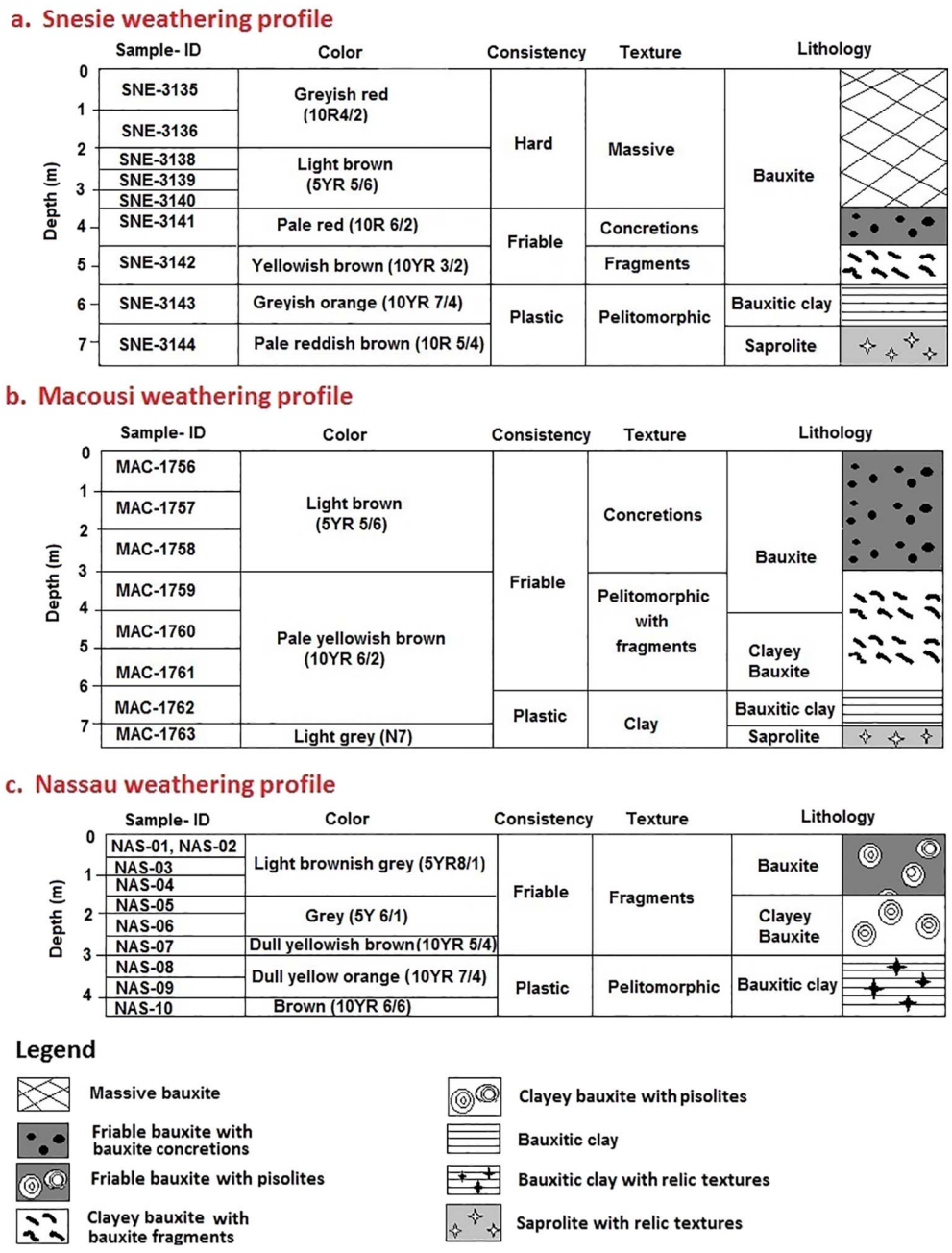

Fig. 3. Weathering profiles of the Snesie drill hole (SNE-10-04), the Macousi drill hole (MAC-10-01) and the Nassau drill hole (PC-10-0131).

maximum width of roughly 13.5 km. The rugged surrounding terrain is also known as the "Brokolonko landscape" (Kroonenberg and Melitz, 1983). The Brownsberg bauxite predominantly occurs on the main plateau as part of a significantly larger laterite cap that covers a long narrow plateau, approximately 500 m a.s.l.

The *Lely Mountains* (04°13′–04°29′N, 54°35′–54°46′W), located near the confluence of the Tapanahony River and Lawa River, are composed of a series of 600 to 700 m high plateaus arranged in an arcuate shape (Fig. 2b). The vegetation mainly consists of high dryland tropical rainforest on the plateaus and slopes, and mountain savannah on the plateaus. The laterite capped plateaus are dissected by incisions of several surrounding creeks. The bauxite reserves range between 7 and 15 Mt., at contents of 46–50% available alumina and 1.4–1.5% SiO_2. The bauxite deposit of the Lely Mountains has long been considered unattractive for processing due to its remote location, relatively high boehmite content and the scattered distribution of small pockets of higher-quality bauxite over 40 km long plateaus (Janssen, 1963, 1979).

3. Materials and methods

3.1. Sample locations and studied materials

The studied sites in the Bakhuis Mountains are the BHP Billiton/Suralco LLC Bakhuis Base Camp (Area 10.1) and the Snesie and Macousi exploration trenches (Area 10.2), while those in the Nassau Mountains are situated on Plateau C (Fig. 2a, b, c). Weathering profiles of the Snesi and Macousi trenches were sampled down to a depth of 7.5 m at vertical intervals of 50-100 cm, based on changes in lithology (Fig. 3). Ten drill cutting samples were collected from Snesie drill hole SNE-10-04 and from Macousi drill hole MAC-10-01. The deepest interval at Snesi

(7.0–7.5 m) had not been recovered during drilling. The Bakhuis Base Camp samples were taken from an outcrop of a high-grade metamorphic rock considered to be the potential parent material of bauxite in the surrounding area. Sample BAK-02 is a relatively fresh piece of crystalline rock, whereas sample BAK-01 is a strongly weathered equivalent. Samples from Nassau were eleven cuttings from drill core PC-10-0131 on plateau C, which were kindly provided by Suralco L.L.C. Major-element XRF data for deposits from Brownsberg, Lely and Nassau Mountains were provided by the Bauxite Institute of Suriname.

3.2. Analytical methods

Mineralogy and microstructures were investigated on polished thin sections of drill cuttings, and rock samples with an optical microscope and an electron microprobe (JEOL JXA-8600 Superprobe) using both energy dispersive (EDS) and wavelength-dispersive (WDS) analytical techniques. Back-scatter electron imaging (BSE) was used to identify mineral phases and to study textural relationships. Quantitative compositions of mineral phases were determined in representative textural domains of selected samples from the Snesie trench, Bakhuis Base Camp and Nassau. X-ray diffraction (XRD) patterns were collected from randomly oriented powder samples using a Bruker D2 Phaser X-ray diffractometer, operated in a step-scan mode, with Co-Kα radiation (1.78897 Å). The counting time was 66 s/step, the step size 0.05° and the range 5–85°. Total acquisition time per sample was approximately 15 min.

Major element compositions were determined by X-ray fluorescence (XRF) on fused glass beads (lithium borate) with a Thermo ARL 9400 sequential XRF (Utrecht University) and a Panalytical MagiXPro XRF (VU University Amsterdam). Loss-on-ignition data were obtained either by measuring weight loss upon heating of a powdered sample in an oven at > 1000 °C or by thermogravimetric analysis (TGA) during which weight loss was continuously monitored over a temperature range between room temperature and 1000 °C. The major-element data provided by Suralco and Bauxite Institute Suriname include values for loss on ignition (LOI), total alumina (TAl_2O_3), available alumina (AA_{143}), total silica ($TSiO_2$) and reactive silica ($RSiO_2$).

Trace elements were determined by laser-ablation inductively coupled mass spectrometry (LA-ICPMS) on the fused glass beads prepared for XRF, using a ThermoFischer Scientific Element 2 magnetic sector instrument, integrated with a Lambda Physik excimer laser (193 nm) with GeoLas optics. Main parameters for the ablation spot setup were: 5 mJ laser energy, 10 Hz pulse repetition rate and 120 μm spot diameter. The ICP-MS operating conditions were plasma power: 1300 W; gas flow rates (L/s): cool-16.0, auxiliary-1.0, sample-0.685, carrier He-0.696, peak-jump scanning mode; time-resolved acquisition mode; 60 s total ablation time. Si was employed as internal standard. SRM NIST-612 was used during the measurements to correct for background and drift with double-standard measurements bracketing each six samples. Reported compositions are averages of three measurements for each sample. Accuracy of the results was monitored by analyzing USGS standard BCR-2 after each six samples. The percentage of deviation from recommended values, determined in multiple sessions, was generally ≤ 10% for all reported trace elements. Results obtained on the ARNT bauxite standard BX-N are given in Appendix A.

4. Results

4.1. Textures and mineralogy

4.1.1. Bakhuis Mountains: Snesie and Macousi

Several different textural/lithological zones were observed in the drill cuttings of the Snesie weathering profile (Fig. 3a). The greyish-red massive hard bauxite top layer passes downwards into a pale-red friable earthy layer consisting of bauxite fragments/concretions and clayey bauxite. This zone then gradually changes into a kaolinite-rich saprolitic horizon with a relic parent-rock structure of alternating light and dark colored bands (Figs. 3, 4a, c). The bauxite of the Macousi trench is generally soft with concretions at the top of the weathering profile, which passes into bauxite fragments in a clayey matrix and finally into a grey saprolite with a similar gneissic foliation as observed at Snesie (Fig. 3b). The most important difference between the bauxite from Macousi and Snesi is its degree of consolidation, as the bauxite from Macousi is mainly soft, while that of Snesie has a very hard top section and becomes softer with depth.

In the Snesie and Macousi weathering profiles, gibbsite is the dominant mineral at the top and kaolinite at the bottom of the weathering profile. Bauxite samples also contained goethite, hematite, ilmenite, and traces of anatase and zircon (Fig. 4a–f, 6). The Al-rich matrix is generally fine grained and porous, while the voids are occasionally lined with coarse grained secondary Al-hydroxides (gibbsite) or iron-(hydr)oxides (hematite and goethite solid solutions) (Fig. 4b, f). EDS analysis revealed that the average Al_2O_3 content of gibbsite in the Snesie samples is 63.7 ± 1.24 wt% (n = 37). The middle friable earthy zone of the profile consists of gibbsite-rich fragments and Fe-rich concretions, which becomes more kaolinite-rich towards the bottom. This change in mineralogy is consistent with the XRD and XRF data from both weathering profiles (Figs. 6a, b and 7). A clayey texture appears at the transition zone around 5 m depth where sample SNE-3142 was taken, which contains substantially more clay than the samples at the top of the profile. Further down, the texture in the samples becomes pelithomorphic (uniform clayey matrix) with a relic foliation of alternating dark and light colored layers and relic blasts from an apparently gneissic parent rock (Fig. 4a, c). These relict are surrounded by pressure shadows and are probably weathered sillimanite blasts that were almost completely converted into gibbsite (Fig. 4c, d). The altered blasts also contain clusters of kaolinite flakes (Fig. 4d). Vermicular kaolinite stacks were observed in the saprolite of the Snesie area. Kaolinite peaks in XRD spectra appeared in samples from approximately 4 m depth, consistent with appearance of the first clusters of kaolinite flakes in sample SNE-3141 and MAC-759. It is possible that small quantities of kaolinite (< 0.5%) are present in the top samples but remained undetected by XRD. The coarse grained Ti-Fe-oxides such as ilmenite and pseudo-rutile generally have a sub- to euhedral shape (Fig. 4e, f). They are occasionally clustered and aligned, showing a preferred orientation which could also be a relic texture (Fig. 4e).

4.1.2. Bakhuis Base Camp

Sample BAK-01 is a severely weathered equivalent of BAK-02, which is a relatively fresh piece of amphibolite with a characteristic preferent mineral orientation. Quartz, gibbsite and Fe-(hydr-)oxides (hematite, goethite) with minor amounts of Ti-oxides (anatase, ilmenite) and zircon are the main phases in BAK-01 (Fig. 4g–l). Quartz grains in BAK-01 showed signs of dynamic recrystallization, corrosion and dissolution (Fig. 4h). The presence of a fresh core with a weathered rim in BAK-02 provided an opportunity to analyze the weathering products and microtextures within and around the altered minerals. Parallel alignment of amphibole (magnesiohastingsite), plagioclase (64% anorthite), orthopyroxene (hypersthene), and quartz constitutes the foliation in BAK-02 (Fig. 4g). Weathering in plagioclase (andesine) and amphibole, started along cleavages and fractures where gibbsite was formed (Fig. 4i, j). Gibbsite is the dominant secondary mineral and its crystals are clustered along septa (threads) forming a boxwork texture (Fig. 4h–k). The thin brown lineaments along the median plane of the septa mark the position of the initial fractures in the precursor feldspar grain (Fig. 4h). Clusters of kaolinite are also present in the weathered rims of the samples (Fig. 4j). The secondary Fe-hydroxides (goethite) that formed after hornblende show a regular boxwork texture

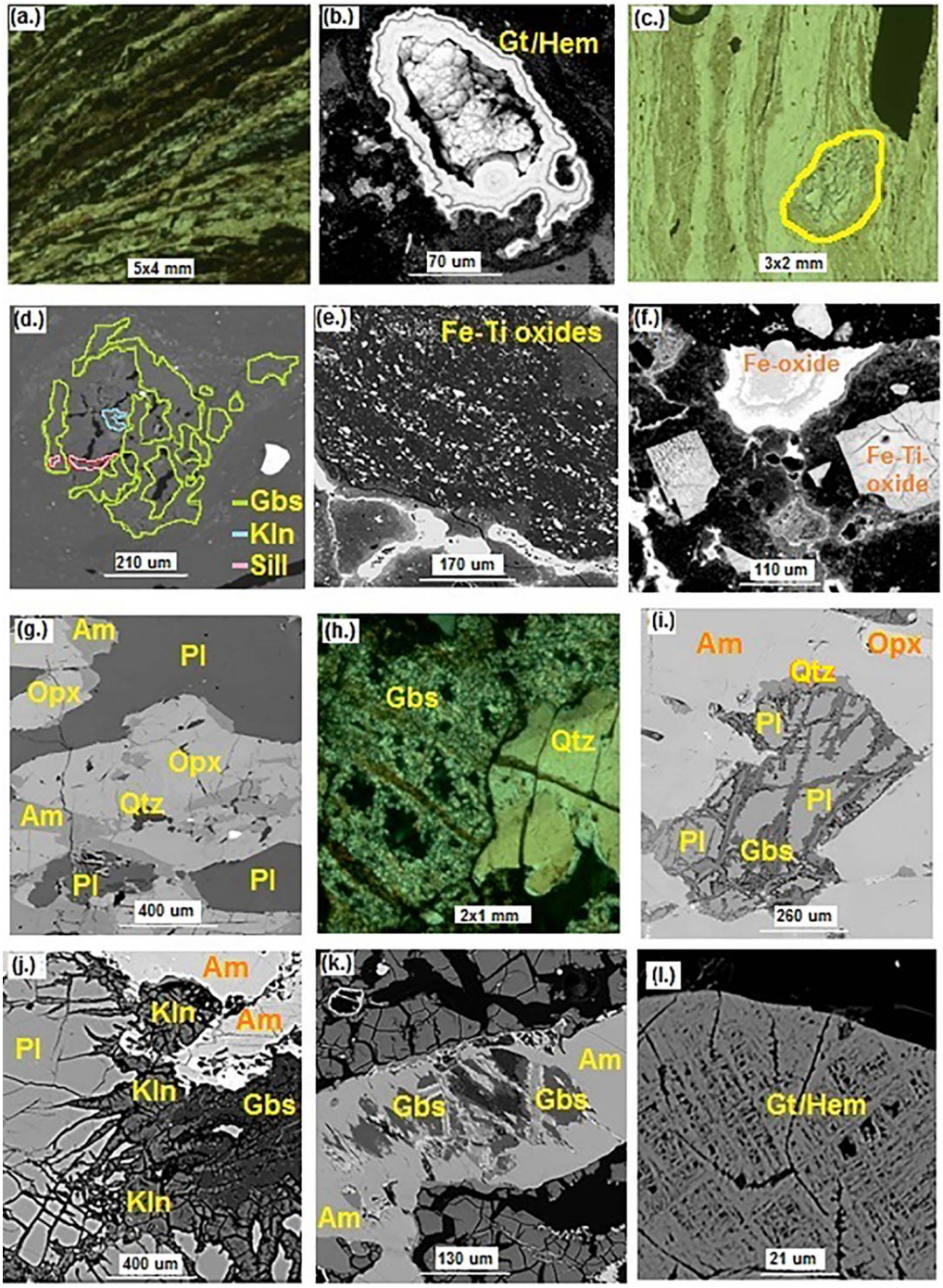

Fig. 4. (a) Optical microscope image of gneissic banding in bottom sample SNE-3144 at 7 m depth (plane polarized light); (b) BSE image of void/geode filled with (Al)-goethite and hematite layers with a botryoidal texture in its center in SNE-3136 at 1.5 m depth; (c) optical microscope image (plane polarized light) of an altered Al-rich relic blast (with yellow outline) and foliation in saprolite sample SNE-3143 at 6 m depth; (d) Enlarged BSE image of an altered blast at 6 m depth where the areas with green outlines represent gibbsite (Gbs), while the pink outlines represent sillimanite (Sill) and the blue outline a kaolinite cluster (Kln); (e) BSE image showing aligned Fe-Ti-oxides (ilmenite) in the Al-rich matrix of SNE-3136; (f) euhedral to subhedral Fe-Ti oxide crystals from the upper part of the weathering profile. The geode in the upper part of the image is filled with iron oxides (SNE3136); (g) BSE image of the unweathered core of outcrop sample BAK-02 consisting of amphibole (Am), orthopyroxene (Opx), plagioclase (Pl) and quartz (Qtz); (h) Optical microscope image (plane polarized light) of a fine grained gibbsite boxwork in outcrop sample BAK-01 growing along brown Fe-rich relict fractures or cleavage planes of plagioclase. Large quartz grain in the right corner; (i) Partially altered plagioclase (andesine) grain with secondary gibbsite along its fractures in BAK-02; (j) BSE image of indirect weathering of plagioclase into gibbsite via kaolinite; (k) Gibbsite in a weathered amphibole grain; (l) Goethite and hematite boxwork formed after hornblende weathering in BAK-01. (For interpretation of the references to color in this figure legend, the reader is referred to the web version of this article.)

or crossed septo-alteromorph (Fig. 4l). Ilmenite, pyrite, zircon, magnetite, apatite and Ni-bearing iron sulfides were present as accessory phases in BAK-02. XRD spectra confirm the presence of the major phases (Fig. 6).

4.1.3. Nassau Mountains (Plateau C)

The cores from the weathering profile in drill hole PC-10-0131 were investigated down to a depth of 4.5 m. The upper part of the bauxite layer (0–3 m) is massive and contains gibbsite, Al-goethite, hematite, and anatase. The massive pisolitic bauxite gradually transforms into a bauxitic clay with a relic parent-rock texture and large amounts of kaolinite in the lowermost 1.5 m (Fig. 5a–d). The pisoliths have concentric layering and occasionally contained variable amounts (0–30%) of ilmenite inclusions In sample NAS-08 a gneissic foliation with alternating dark and light colored layers was observed. The most dominant mineral in the Nassau bauxite samples is gibbsite, followed by Al-rich iron-(hydr-) oxides (goethite and hematite) and minor amounts of Ti-Fe-oxides (ilmenite), boehmite, and quartz (Fig. 6 and Table 1). Coarse euhedral and subhedral authigenic gibbsite crystals with numerous twins line the voids and constitute the matrix (Fig. 5d, e). Some voids are marked by a primary lining of euhedral gibbsite crystals which is coated with a layer of goethite (Fig. 5e).

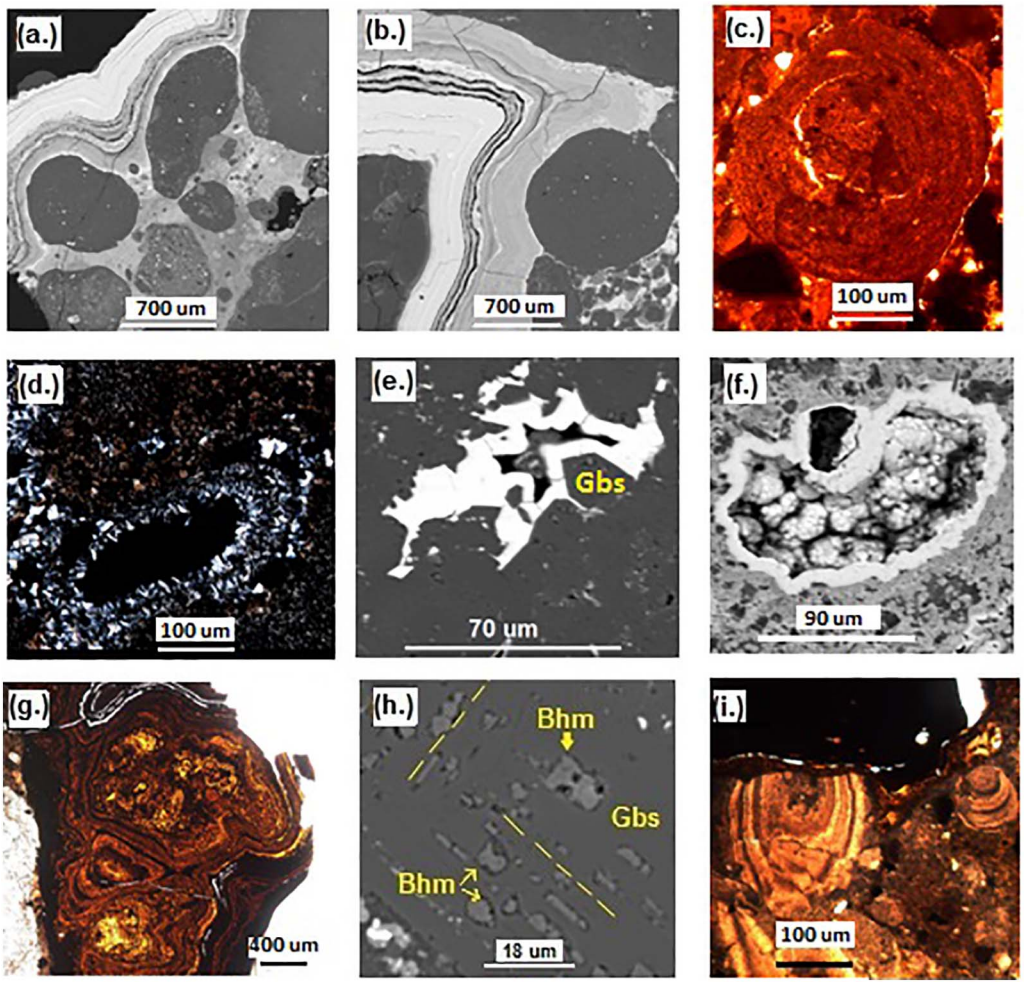

Fig. 5. (a) BSE image of the pisolithic bauxite with alternating Al-hematite and Al-goethite layers (NAS-03); (b) BSE picture of an gibbsite-rich pisolith and cyclically precipitated iron oxide layers (NAS-03); (c) microscope image of an iron stained gibbsite-rich pisolith with concentric layering (NAS-03); (d) microscope image of double gibbsite lining (NAS-grey); (e) BSE image of a void with euhedral gibbsite crystal lining (grey), coated with goethite (white); (f) BSE image of geode filled with goethite crystals showing a botryoidal texture (NAS-08); (g) Microscope image of multiple concentric Fe-oxide linings (PPL); (h) BSE image of boehmite (Bhm) crystals with a parallel orientation determined by two cleavage planes of a precursor mineral, resulting in a cross pattern. The surrounding dark grey material consists of gibbsite (Gbs) (NAS-11); (i) Microscope image of an illuvial textures in NAS-03 (PPL).

In some samples (e.g., NAS-03) yellow/reddish brown goethite and hematite banding was observed lining voids, surrounding concretions or forming a botryoidal texture within voids (Fig.5a, b, e–g). EDS analysis revealed Al substitution (1–16 wt%) in goethite and hematite in these layers. Sample NAS-11 contains an intergrowth of gibbsite and minor boehmite, with the latter forming a cross linear pattern (Fig. 5h). Several illuviation cutans are present, which result from absolute chemical, mechanical, or biological accumulation of mobile substances previously removed from the corresponding eluvial domain at the top of the profile (Fig. 5i). These illuviation cutans provide evidence for the movement of significant matter at a microscopic scale.

4.2. Geochemistry

Major element data from the Snesie, Macousi, Nassau Mountains, Lely Mountains and Brownsberg exploration drill holes are summarized in Table 2, and complete major and trace element data sets for the profiles that were investigated in detail are reported in Table 3a–3b. Examples of concentration trends in vertical profiles are shown in Fig. 7 and a more extensive illustration of local variability in Appendix B.

The average compositions of drill-hole material from these areas are quite coherent, with total Al_2O_3 ranging between 40 and 49 wt%, except for the Lely Mountains where average Al_2O_3 is only 33 wt%. Average SiO_2 contents are highest at Brownsberg (13 wt%) and lowest at Lely Mts. (6 wt%), whereas Fe_2O_3 contents are highest at Lely Mts. (34 wt%) and lowest at Macousi (13 wt%). The Nassau, Lely and Brownsberg areas stand out in having considerably higher TiO_2 contents (ca. 4–4.5 wt%) than the Snesie and Macousi deposits (ca. 1.6 wt %).

Vertical chemical profiles have many characteristics in common but show differences and considerable local variation in detail. In the more complete profiles, the Al_2O_3 contents often increase first from the saprolitic bottom upwards until reaching a maximum in the bauxite horizon, and then decrease in the duricrust towards the top, as is best illustrated in the Macousi profiles (Fig. 7 and Appendix B). The Al_2O_3 maxima mark the level where SiO_2 reaches lowest concentrations after a steady upwards decline, and where Fe_2O_3 starts to increase in the top interval. In the Snesie (-3 to -5 m), Macousi (-3 to -4 m) and Lely Mts. (-3 to -4 m) profiles, this inflexion point, where SiO_2 reaches lowest concentrations, generally lies deeper than in the Nassau (<1 to 4 m) and Brownsberg (ca. -2 m) profiles. At Snesie, the depth of the Al_2O_3 maxima roughly coincides with a transition from friable bauxite to a more massive bauxite, whereas at Macousi it corresponds to a transition from a clayey bauxite to friable bauxite. The uppermost part of the Snesie profiles is relatively complex in showing more fluctuations, in agreement with the presence of an additional top layer of massive bauxite (Fig. 3). The LOI values mirror those of Al_2O_3, independent of the colour change, whereas Fe_2O_3 shows opposite

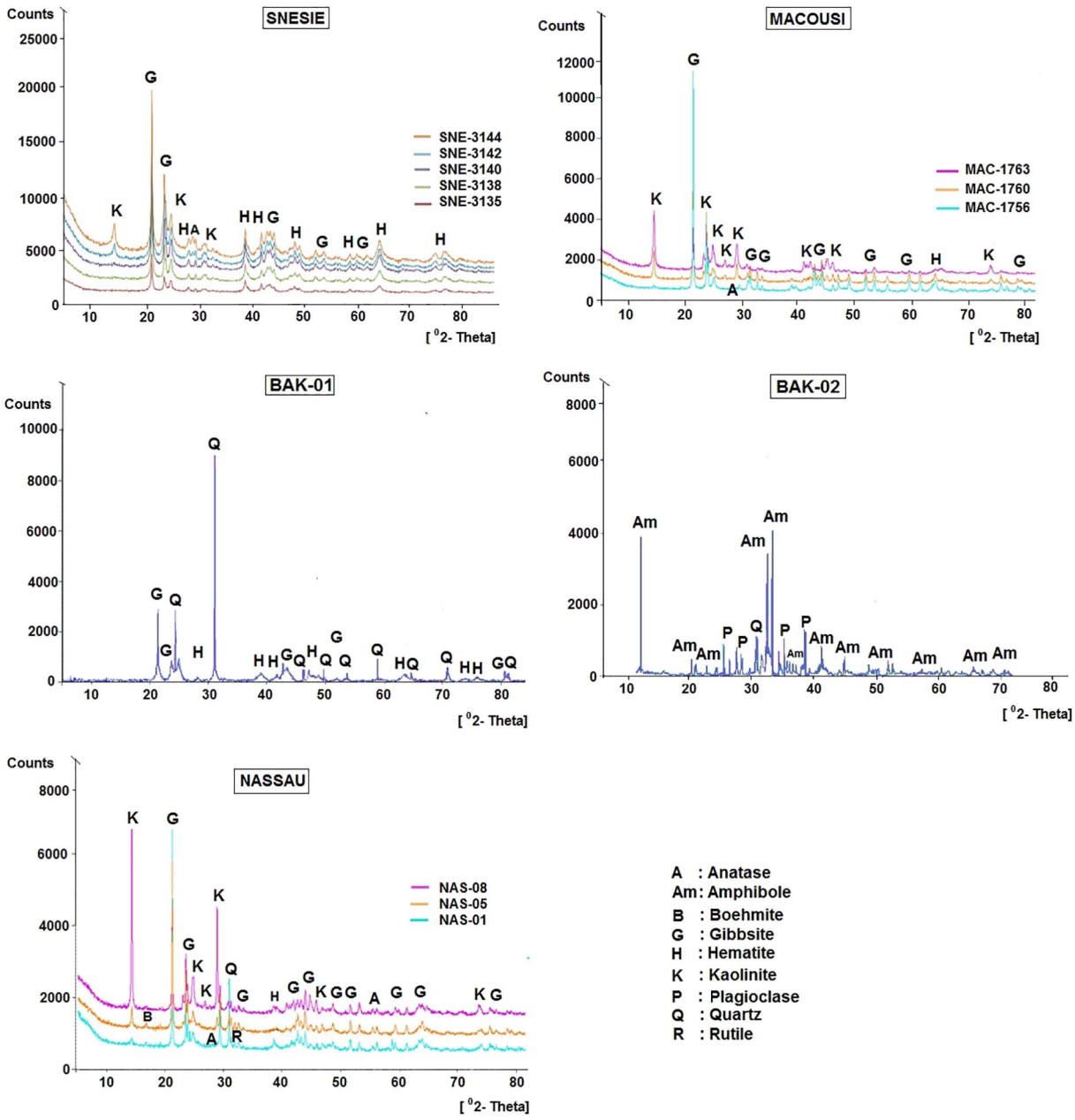

Fig. 6. X-ray diffraction patterns of a select group of samples from the Bakhuis- and Nassau study locations. The spectra reveal the changing mineralogy in the weathering profiles with depth.

Table 1
Compilation of the mineralogy for selected samples from the study areas. Estimated abundancies are based on XRD, electron microprobe and microscopic analysis.

	SNE-3135	SNE-3140	SNE-3144	BAK-01	BAK-02	NAS-01	NAS-03	NAS-08	MAC-1756	MAC-1760	MAC-1763
Gibbsite	+ + +	+ + +	+	+	—	+ + +	+ + +	+	+ + +	+ + +	+
Boehmite	—	—	—	—	—	+ +	+	—	—	—	—
Hematite	+ +	+ +	+	+	—	+ +	+	—	+ +	+	—
Goethite	+	+	—	—	—	+	+	—	+	+	—
Kaolinite	—	+	+ + +	+	—	—	—	+ +	—	+	+ + +
Quartz	—	—	—	+ +	+	+	+	+	—	—	—
Anatase	+	—	—	—	—	+	+	+	+	+	—
Amphibole	—	—	—	—	+ + +	—	—	—	—	—	—
Pyroxene	—	—	—	—	+ + +	—	—	—	—	—	—
Plagioclase	—	—	—	—	+ + +	—	—	—	—	—	—
Zircon	+	+	+	+	+	+	+	+	+	+	+

Dominant (+ + +); abundant (+ +); detected (+); absent (—).

Table 2
Concentration averages and standard deviations for LOI and main oxides determined in samples from exploration cores from the Bakhuis area (Snesie and Macousi), Nassau Mountains (Plateau C), Lely Mountains and Brownsberg. Values in wt%. n = number of samples. Data source: Suralco and Bauxite Institute Suriname.

	Snesie	Macousi	Nassau Mountains (Plateau C)	Lely Mountains	Brownsberg
LOI	21.7 ± 4.3	25.6 ± 4.5	22.3 ± 5.9	17.2 ± 5.18	22.4 ± 5.6
SiO_2	9.7 ± 11.5	10.4 ± 10.9	8.4 ± 11.6	6.1 ± 7.71	13.1 ± 12.4
Al_2O_3	40.5 ± 5.0	48.7 ± 5.9	43.5 ± 12.2	33.2 ± 9.67	43.3 ± 8.2
Fe_2O_3	25.3 ± 9.8	12.8 ± 5.53	21.2 ± 18.9	34.1 ± 13.6	16.5 ± 9.4
TiO_2	1.65 ± 0.5	1.5 ± 0.75	3.9 ± 1.8	4.6 ± 2.1	4.0 ± 1.4
n	55	44	1368	3132	488

behavior, as it increases towards the top of the weathering profiles. The TiO_2 contents tend to increase towards the higher parts throughout, which is most obvious in the Nassau and Brownsberg profiles. There is also a steady increase in P_2O_5 contents. The oxides of Ca, Mg, Na and K are depleted along the entire length of the profiles.

Trace-element trends in the investigated Snesie (SNE-10-04) and Macousi (MAC-10-01) profiles display considerable concentration variations and also show distinct patterns in the intervals above and below the transition zone (Fig. 8). Virtually all of the trace elements analyzed are 2–10 times enriched in the top layer relative to the lower parts. Although the chemical variations in the two profiles are not identical, some systematics can be observed in relationships between trace elements and more abundant constituents. Many trace elements show conspicuous increases from the saprolite towards the top of the weathering profiles, followed by a modest decline in the top layer. The most prominent examples are Nb, Ta, REE, Y, Sr, Th, Pb, whereas Zr, Hf, U and Cr show an upward increase throughout. The trends for V and As are similar to those of Fe_2O_3 and P_2O_5. The Snesie profile is more complex than the Macousi profile, in particular since TiO_2 and associated elements (Nb, Ta, REE, Y, Sr) show a double peak. In the

Table 3a
Major oxide (XRF) and trace-element (LA-ICPMS) contents of samples from drill hole SNE-10-04 (Snesie) and Bakhuis Base Camp (n.d.: not detected).

	Snesie										Bakhuis Base Camp	
	SNE3135	SNE3136	SNE3137	SNE3138	SNE3139	SNE3140	SNE3141	SNE3142	SNE3143	SNE3144	BAK01	BAK02
SiO_2 (wt%)	0.50	0.56	1.17	1.74	1.33	3.27	16.34	23.73	30.67	29.19	24.87	51.81
Al_2O_3	41.86	37.56	39.10	45.11	51.22	43.06	47.75	47.32	40.26	42.87	29.37	16.20
TiO_2	2.69	3.17	3.52	2.70	2.81	2.58	3.49	3.01	2.04	2.16	1.36	0.53
Fe_2O_3	31.45	37.18	33.86	25.20	17.03	27.71	9.30	4.48	9.74	7.04	26.93	9.19
MnO	0.017	0.021	0.020	0.012	0.009	0.010	0.013	0.011	0.014	0.010	0.013	0.125
CaO	0.037	0.038	0.042	0.041	0.038	0.036	0.049	0.049	0.047	0.049	0.046	9.97
MgO	0.007	0.033	0.042	0.021	0.010	0.020	0.029	0.017	0.036	0.039	0.026	8.27
Na_2O	0.031	0.030	0.028	0.025	0.025	0.017	0.033	0.017	0.029	0.020	0.043	3.04
K_2O	0.010	0.004	0.006	0.007	0.006	0.006	0.010	0.006	0.009	0.008	0.015	0.23
P_2O_5	0.26	0.27	0.22	0.17	0.13	0.14	0.09	0.08	0.07	0.07	0.10	0.13
LOI	23.14	21.13	21.99	24.97	27.40	23.16	22.89	21.29	17.08	18.54	17.23	0.52
Sum	100	100	100	100	100	100	100	100	100	100	100	100
Sc (ppm)	10	15	15	13	14	20	17	13	17	14	21	34
V	805	840	1037	746	646	1005	523	263	546	374	526	184
Cr	256	329	370	377	345	342	267	173	94	169	456	627
Zn	35	58	30	23	23	29	35	31	41	36	33	109
As	9.2	12	11	12	8.8	12	4.0	2.2	3.1	3.5	8.2	0.8
Rb	0.3	0.2	n.d.	n.d.	n.d.	n.d.	0.2	0.1	0.3	0.4	0.8	0.6
Sr	30	38	44	26	29	28	36	28	11	19	10	265
Y	3.0	4.7	5.0	3.0	3.7	4.0	6.4	4.3	1.4	2.7	2.9	13.2
Zr	142	159	178	146	167	162	158	82	32	50	634	49
Nb	12	13	15	13	12	12	12	7.4	2.0	4.2	13	2.5
Ba	723	79	63	46	39	33	40	36	34	28	14	140
La	23	38	31	19	24	24	34	27	10	17	5.9	18
Ce	39	61	60	39	39	40	65	57	19	35	9.4	21
Pr	4.9	8.2	7.0	4.3	4.9	5.0	7.9	6.8	2.5	4.4	1.1	2.4
Nd	18	32	27	15	19	19	31	25	10	16	3.6	10
Sm	2.82	5.35	4.69	2.31	3.10	3.10	5.05	3.79	1.37	2.33	0.65	2.12
Eu	0.74	1.48	1.30	0.73	0.89	0.93	1.84	1.28	0.40	0.66	0.12	0.75
Gd	1.77	3.19	2.86	1.59	1.94	2.01	3.64	2.20	0.67	1.25	0.41	2.12
Tb	0.22	0.36	0.34	0.18	0.23	0.25	0.41	0.24	0.08	0.16	0.09	0.31
Dy	1.10	1.88	1.76	0.96	1.30	1.27	2.09	1.15	0.48	0.91	0.58	2.16
Ho	0.15	0.28	0.26	0.16	0.20	0.20	0.33	0.18	0.07	0.11	0.12	0.43
Er	0.41	0.61	0.60	0.40	0.48	0.45	0.65	0.40	0.20	0.24	0.47	1.32
Yb	0.38	0.56	0.44	0.36	0.46	0.42	0.54	0.33	0.17	0.23	0.63	1.40
Lu	0.05	0.07	0.07	0.05	0.07	0.06	0.07	0.04	0.02	0.03	0.10	0.22
Hf	4.0	4.4	4.8	3.9	4.9	5.1	4.7	2.5	1.0	1.4	14.6	1.3
Ta	0.7	0.8	0.9	0.8	0.8	0.8	0.7	0.5	0.1	0.3	0.7	0.1
Pb	7.6	9.7	10.7	9.6	9.1	10.3	9.6	6.8	3.2	5.0	5.5	1.1
Th	7.7	10	13	14	16	16	14	7.3	1.7	3.8	6.7	0.05
U	0.7	0.8	1.0	1.1	0.8	0.9	0.6	0.4	0.3	0.3	1.4	0.0

Table 3b
Major oxide (XRF) and trace-element (LA-ICPMS) contents of samples from drill holes MAC-10-01 (Macousi) and PC-10-0131 (Nassau plateau C) (n.d.: not detected).

	Macousi								Nassau			
	MAC-1756	MAC-1757	MAC-1758	MAC-1759	MAC-1760	MAC-1761	MAC-1762	MAC-1763	NAS-03	NAS-05	NAS-07	NAS-08
SiO_2 (wt%)	2.60	3.09	2.51	3.82	11.46	29.06	22.39	34.26	1.29	6.28	9.43	17.62
Al_2O_3	46.57	53.76	56.24	56.30	52.31	44.01	48.35	41.49	52.74	45.92	41.57	35.13
TiO_2	2.18	2.46	2.39	2.18	1.50	0.63	0.98	0.45	7.24	9.20	5.29	5.19
Fe_2O_3	22.15	11.36	8.33	7.57	8.26	7.08	5.95	6.47	12.10	14.27	22.75	24.75
MnO	0.015	0.015	0.013	0.011	0.007	0.002	0.004	0.002	0.060	0.083	0.035	0.041
CaO	n.d.	n.d.	0.001	0.001	n.d.	n.d.	n.d.	n.d.	n.d.	0.000	n.d.	n.d.
MgO	0.014	0.006	0.003	0.001	n.d.	0.000	0.000	0.002	n.d.	0.020	n.d.	0.003
Na_2O	0.007	0.004	0.010	0.006	0.006	0.007	0.006	0.005	0.011	0.008	0.004	0.007
K_2O	0.011	0.012	0.012	0.011	0.009	0.009	0.009	0.008	0.008	0.028	0.005	0.007
P_2O_5	0.08	0.04	0.04	0.03	0.03	0.01	0.02	0.01	0.09	0.08	0.04	0.04
LOI	26.37	29.26	30.45	30.08	26.42	19.19	22.28	17.30	26.46	24.11	20.88	17.20
Sum	100	100	100	100	100	100	100	100	100	100	100	100
Sc (ppm)	14	11	10	10	9	8	8	10	22	30	43	51
V	1343	606	427	423	385	242	220	198	1240	1207	1916	1601
Cr	749	676	666	651	555	391	389	323	954	895	569	440
Zn	26	24	22	21	22	28	25	17	49	58	26	32
As	23	12	9.3	8.8	8.7	4.6	4.7	3.7	26	29	20	16
Rb	0.4	0.3	0.3	0.2	0.3	0.4	0.3	0.4	0.3	1.5	0.2	0.2
Sr	23	30	31	30	22	9	15	5	19	35	14	13
Y	7.0	8.4	8.1	7.6	5.2	2.2	3.4	1.5	12	21	7.6	7.5
Zr	299	284	273	239	154	64	105	42	863	1082	498	479
Nb	21	26	26	25	17	7	11	5	55	72	38	32
Ba	13	16	17	17	13	14	12	12	9.2	23	7.5	8.3
La	25	30	31	31	24	14	21	21	22	34	20	19
Ce	29	38	40	39	28	12	19	8	27	47	21	19
Pr	3.5	4.6	4.7	4.6	3.3	1.4	2.2	0.9	2.9	5.0	2.3	2.1
Nd	12	16	17	17	12	4.8	7.6	3.1	10	18	8.0	7.1
Sm	2.07	2.69	2.70	2.60	1.83	0.75	1.22	0.43	1.55	2.97	1.22	1.24
Eu	0.47	0.59	0.62	0.61	0.39	0.18	0.29	0.11	0.31	0.62	0.28	0.26
Gd	1.37	1.83	1.74	1.72	1.26	0.50	0.85	0.33	1.29	2.44	0.86	0.94
Tb	0.20	0.25	0.25	0.25	0.15	0.07	0.11	0.04	0.20	0.41	0.14	0.14
Dy	1.31	1.64	1.58	1.56	1.01	0.45	0.70	0.29	1.62	3.08	1.10	1.12
Ho	0.25	0.31	0.30	0.28	0.19	0.09	0.14	0.06	0.40	0.69	0.27	0.27
Er	0.77	0.93	0.88	0.86	0.60	0.26	0.39	0.18	1.57	2.57	1.02	1.04
Yb	0.87	1.01	1.03	0.97	0.66	0.31	0.48	0.21	2.78	4.44	1.90	1.84
Lu	0.14	0.17	0.16	0.14	0.10	0.04	0.06	0.04	0.61	0.93	0.43	0.42
Hf	6.9	6.8	6.7	6.0	4.0	1.7	2.7	1.1	20	25	12	12
Ta	1.2	1.5	1.6	1.5	1.0	0.4	0.7	0.3	3.2	4.3	2.3	1.9
Pb	9.2	10.1	10.4	10.9	8.2	4.4	6.0	3.3	10.5	18.3	9.9	9.0
Th	14	16	17	18	14	5.9	9.5	4.0	23	23	12	13
U	1.4	1.4	1.3	1.3	0.9	0.5	0.7	0.4	1.9	3.0	1.5	1.5

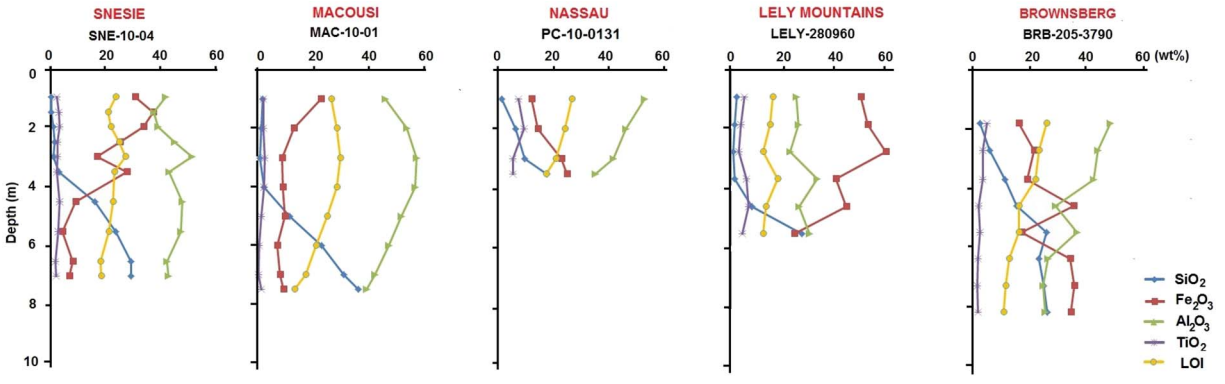

Fig. 7. Examples of vertical variations of major-element contents in weathering profiles from drill holes in the Bakhuis area (Snesie and Macousi), Nassau Mountains, Lely Mountains and Brownsberg. More extensive illustrations are shown in Appendix B.

relatively short Nassau profile (ca. 4 m) analyzed for major and trace elements, Sc and V decrease along with SiO_2 and Fe_2O_3 towards the top, while Cr increases together with Al_2O_3. The pattern for TiO_2 is somewhat irregular and is largely mimicked by Zr, Nb, Ta, REE, Y and Sr.

The results for the two samples from the Bakhuis Base Camp location trace the compositional change between a fairly 'fresh' metamorphic parent rock (BAK-02) and a strongly weathered lateritic equivalent (BAK-01). Compared to the parent rock, the laterite is

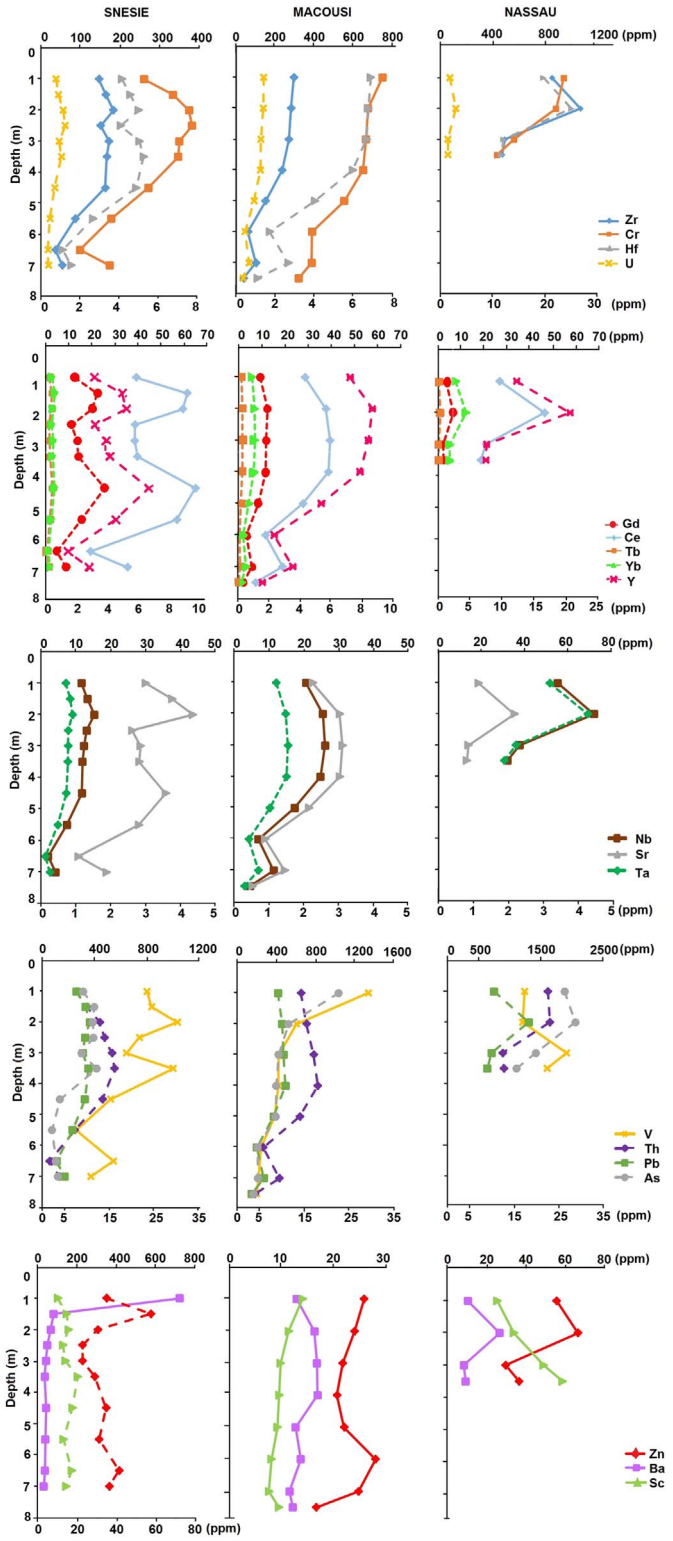

Fig. 8. Vertical concentration changes for selected trace elements in Snesie, Macousi and Nassau profiles. X-axes at the top of the panels are valid for the full lines and those at the bottom for the dashed lines.

enriched in Al_2O_3, Fe_2O_3, and TiO_2, has lower SiO_2 and is strongly depleted in Na_2O, K_2O, CaO, MgO and MnO. BAK-01 contains higher concentrations for Zr, Hf, Nb, Ta, Pb, Th, U, V, As, whereas other trace elements are depleted relative to BAK-02.

5. Discussion

5.1. Formation of weathering products and textural features

5.1.1. Main weathering minerals

5.1.1.1. Gibbsite and boehmite. This study confirms previous observations that gibbsite is the main Al-hydroxide in the Bakhuis and Nassau bauxite deposits (Pollack, 1983; Billiton, 1979; Bárdossy and Aleva, 1990; Janssen, 1963, 1977, 1979). Based on morphological textures (cf., Delvigne, 1998), two different generations of gibbsite can be distinguished in the samples. The first generation is represented by:

(a) Aphanitic to coarse grained gibbsite-rich matrix (crypto-alteromorphs) after kaolinite (4j);
(b) Coarse grained septa forming a glomero-septo-alteromorph after feldspar (4 h, i), while the second-generation gibbsite appears as:
(c) Coarse grained void linings/coatings (Fig. 5d, e).

This generation of gibbsite originated from the precipitation and aging of colloidal Al-rich solutions migrating in the bauxite horizon and in the duricrust. Multiple gibbsite linings in voids and the perpendicular orientation of grains against the walls of voids and pores are consistent with an allochthonous origin of the mineral, also known as allogenic deposit (Bárdossy and Aleva, 1990; Delvigne, 1998).

Boehmite is only a minor phase in the Nassau and Bakhuis deposits, and its presence has also been reported for the bauxite deposits of Brownsberg and the Lely Mountains (Van Kersen, 1956; Janssen, 1963, 1979). The microtextures in the Bakhuis and Nassau samples thus suggest that gibbsite and boehmite are products of one or more of the following reactions:

1. Direct conversion of feldspar (plagioclase) into gibbsite or boehmite.

Gibbsite septa and aligned boehmite following fossil cleavage patterns or irregular transmineral fractures signal this mechanism (Figs. 4h–l, 5h). Next to gibbsite, it is conceivable that boehmite locally originated as a primary weathering product as well. Direct formation from the dissolution of feldspar (Helgeson, 1971; Pollack, 1981; Bárdossy and Aleva, 1990; Kawano and Tomita, 1995 and references therein) would be generally consistent with the nature of the parent rocks at Nassau and Bakhuis.

2. Gibbsite as desilication product of kaolinite

Transformation of kaolinite into gibbsite (following the conversion of plagioclase into kaolinite; Fig. 5e) is described by the reaction:

$$Al_2Si_2O_5(OH)_4 + H_2O \rightarrow 2Al(OH)_3 + 2SiO_2(aq)$$

Continuous plagioclase weathering into kaolinite can also give rise to the formation of boehmite by incongruent dissolution:

$$Al_2Si_2O_5(OH)_4 \rightleftarrows 2AlO(OH) + 2SiO_2(aq) + H_2O$$

These desilication reactions are a function of silica and water activity, humidity, depth to the water table and the presence of other ions (Tardy, 1997; Zhu et al., 2006; Wei et al., 2014).

3. Dehydration of gibbsite into boehmite

Gibbsite, usually the primary Al-hydroxide mineral to form during bauxitization of water-rich, iron-poor systems (Saalfeld, 1958; Zhu et al., 2010), may later dehydrate into boehmite (Trolard and Tardy, 1987; Gong et al., 2002). A decrease in water activity, high surface temperatures and dry conditions during the dry seasons either facilitates this dehydration reaction or establishes thermodynamic conditions where boehmite is the main crystallizing phase instead of gibbsite (Trolard and Tardy, 1987; Eggleton and Taylor, 2008 with references

therein). The possible presence of mixed crystals, resulting from isomorphous replacement or intergrowth (Gong et al., 2002), could not be ascertained because of the small grain sizes of the Al-oxides in the matrix.

4. Direct conversion of pyroxene/amphibole into gibbsite.

This reaction represents a separate type of weathering mechanism, involving direct transformation of framework silicate minerals into the layered Al-OH structure of gibbsite (Valeton, 1972; Aleva, 1994; Dos Muchangos, 2000).

5.1.1.2. Hematite and goethite. Hematite (red, grey, black) and goethite (yellow, brown) are both present as mottles, nodules, botryoidal voids fillings, finely dispersed in kaolinitic matrix or as alternating rims enveloping pisoliths. The broad goethite and hematite peaks in the XRD spectra (Fig. 6) suggest either that not a single, uniform phase is present in the samples but a range of compositions resulting from solid solution, as was also reported for other Surinamese bauxites (Feret et al., 1997), or that crystallinity is poor. Hematite generally forms away from voids and channels with circulating water, where goethite is the dominant mineral (Tardy, 1997). The goethite linings and voids fillings (Fig. 5a, b, e, f, g), reflect cyclic iron dissolution and precipitation by redox or pH alternations that drive iron away from reducing towards oxidizing areas (Topp et al., 1984; Scott and Pain, 2009). The redox changes are probably linked to fluctuating groundwater in the mottled horizon of Nassau Plateau C, where aquifers are strongly affected by the alternating dry and wet seasons.

The available EDS results point to substantial amounts of Al_2O_3 in goethite (ca. 16 wt%) and hematite (ca. 2 wt%) in the Nassau and Bakhuis samples, in accord with the generally lower Al-substitution in hematite than in goethite (Fitzpatrick and Schwertmann, 1982; Tardy and Nahon, 1985; Trolard and Tardy, 1987). Earlier work reported 20–25 wt% Al_2O_3 substitution into goethite from the Bakhuis bauxite deposit (Billiton, 1979). Commonly, the Al_2O_3 contents in hematite and goethite increase towards the top of weathering profiles (Trolard and Tardy, 1987), apparently reflecting the amount of available Al in solution. Hence, high Al-substitution in goethite is found when the mineral is associated with gibbsite or boehmite.

5.1.1.3. Kaolinite. Kaolinite was mainly observed in the bottom parts of the weathering profiles. Its absence in the bauxite layer can be attributed to a slow crystallization reaction of kaolinite relative to gibbsite formation. This facilitates removal of freshly formed SiO_2-rich colloids by draining solutions, essential for gibbsite stability (Schellmann, 1994 and references therein). The large kaolinite quantities at the bottom of the profiles have a negative impact on the drainage and leaching conditions at depth. Early-formed kaolinite in laterite and bauxite, produced from the weathering of primary silicates in parent rock, is often dissolved and replaced by a second generation of kaolinite with lower crystallinity and higher iron content (Schellmann, 1994 and references therein). The dissolution of kaolinite could be promoted by release of protons caused by ferrolysis (Nahon and Merino, 1997). The quantity of secondary kaolinite increases during lateritization. The observed textures point to a similar complex history for kaolinite in the studied weathering profiles. In all of the samples, neo-formed iron-stained kaolinite has a smaller grain size and fills voids in the matrix.

5.1.2. Origin and evolution of secondary textures

5.1.2.1. Origin of void fillings. The gibbsite and goethite crystallaria and clay illuvia observed in veins and voids of the Bakhuis and Nassau samples formed by different mechanisms. The crystallaria nucleated on the walls of voids in the matrix, and grew perpendicular to these from

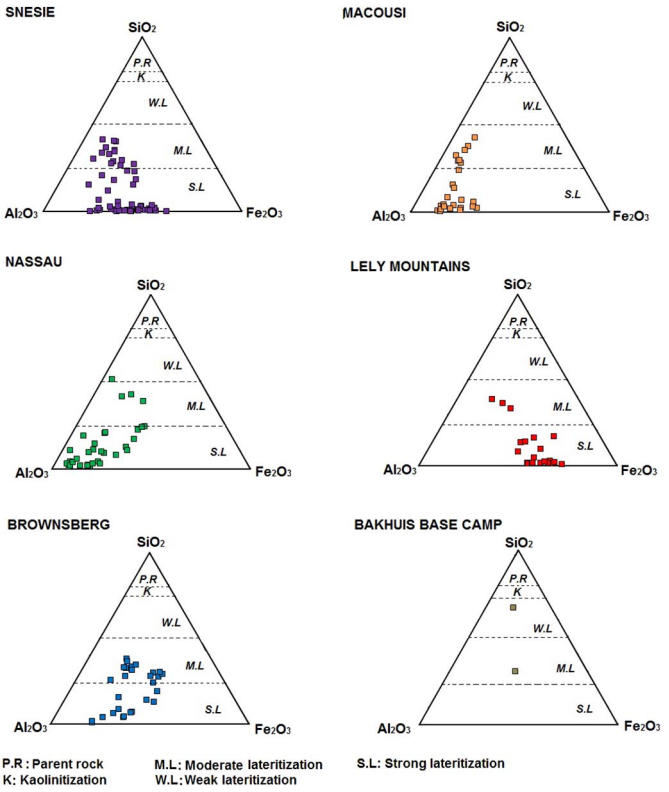

Fig. 9. Triangular plots depicting the degree of lateritization in all study areas (diagram based on Schellmann, 1983, 1986).

passing Fe or Al-rich solutions, whereas transport of detrital material (illuvium) produced void linings that tend to be layered or microstratified parallel to the walls (Delvigne, 1998; Velde and Meunier, 2008). Goethite and gibbsite crystallaria in voids can also be a result of in-situ degradation of ferro-argillans previously deposited from suspensions of clay microparticles, but then the crystals should be lined parallel to the walls as well (Delvigne, 1998). The gibbsite-filled void with goethite lining in the Nassau sample (Fig. 5h) demonstrates that both Al and Fe were mobile at some point and that initial formation of gibbsite crystals was followed by a goethite lining. Both elements were probably transported through the soil system by oscillating groundwater, which could also have induced fluctuations in chemical conditions favorable for dissolution-deposition sequences. The percolating water removes soluble substances, while evaporation brings dissolved components to the surface by capillarity (Scott and Pain, 2009). The ongoing wetting and drying cycle in the Nassau deposit from oscillating groundwater creates cracks during dry seasons and their re-filling with gibbsite, goethite or clay minerals during wet seasons. Illuviation textures (cutans) in the Bakhuis and Nassau samples are made up of amorphous clay minerals (kaolinite-group minerals), which points to clay migration within the profiles at each of these locations (Fig. 5i). This filling of cracks and voids with clay minerals may have influenced the composition of the resulting bauxite, and it also reduced its porosity and permeability.

5.1.2.2. Evolution of pisoliths and concretions. The most prominent textural difference between the Bakhuis and Nassau bauxite is the abundance of hematite, goethite and gibbsite pisoliths in the latter, some of which showing concentric zonation (Fig. 5c). Pisoliths can form under various specific conditions. Precipitation of Al and Fe-hydroxide tends to form rounded pedological features, driven by the material's

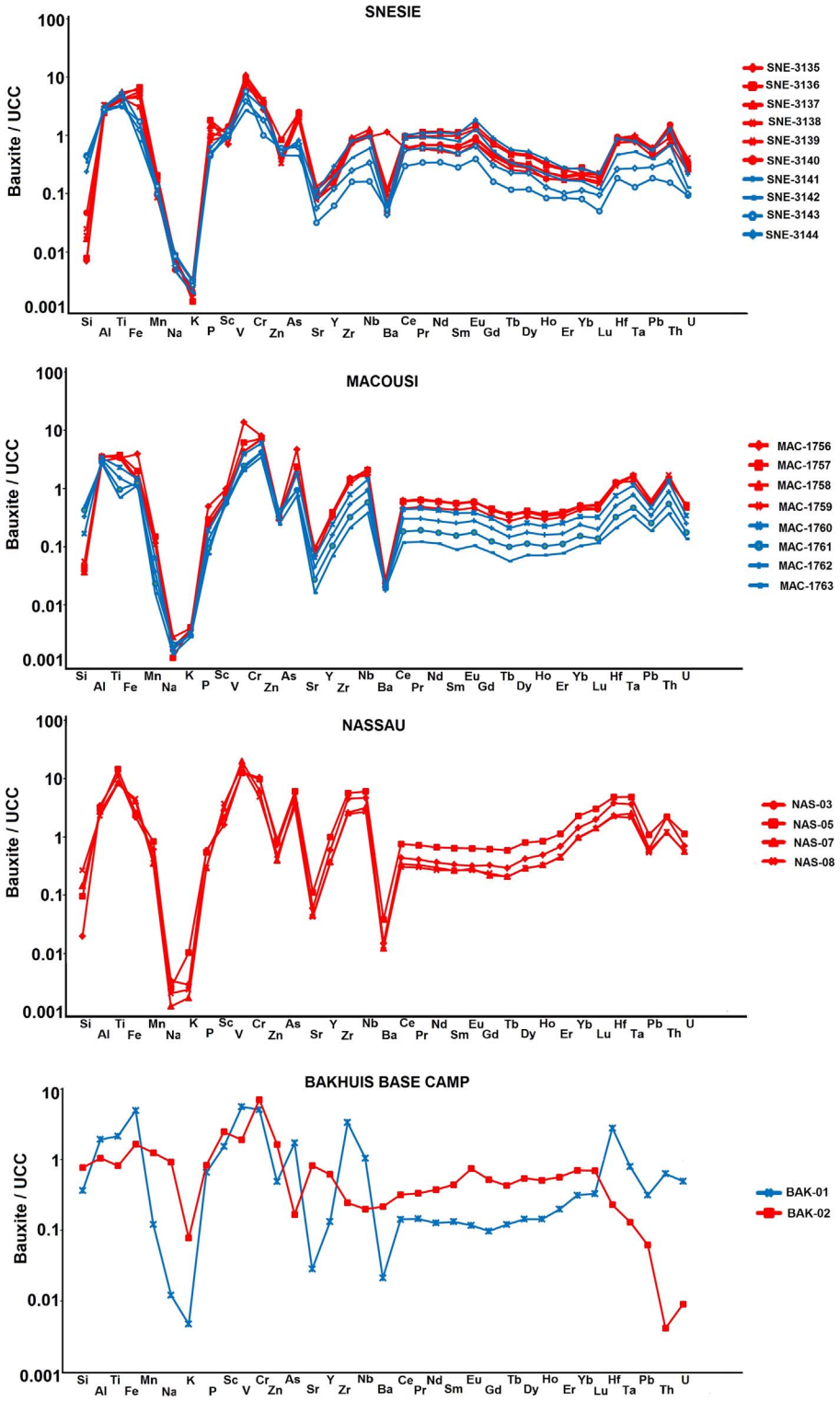

Fig. 10. (Upper-continental-crust (UCC) normalized element distributions in the studied weathering profiles. Samples indicated in red have < 5 wt% SiO_2, while those in blue contain > 5 wt% SiO_2. Ca and Mg are not indicated as their concentrations are extremely low and often remained below detection limits for XRF analysis. Note the strong depletion of fluid-mobile elements and the contrasts in the REE part of the patterns for the different areas. (For interpretation of the references to color in this figure legend, the reader is referred to the web version of this article.)

tendency to form shapes with minimum specific surfaces, as is well known from other studies (Tardy and Nahon, 1985; Bárdossy and Aleva, 1990; Taylor and Eggleton, 2008; Wei et al., 2014). Iron mottles are often associated with kaolinite in mottled zones (Tardy, 1997) where they may evolve into Al-hematite-rich concretions that are subsequently dehydrated into Al-goethite along the rims (Tardy and Nahon, 1985). The segregation of Al and Fe in pisoliths and concretions can also result from outward migration of the iron. Fe-rich coatings around concretions are produced by absorption or precipitation of migrating iron. Delvigne (1998) attributed the formation of pisolitic bauxite to degradation under fluctuating chemical conditions, accompanied by the formation and evolution of glaebules at the expense of either isalteritic or alloteritic bauxite. The fluctuating groundwater table and plateau-shaped landscape of the Nassau Mountains have a significant influence on hydration control, since alternations of hydration, drainage and redox conditions are favorable

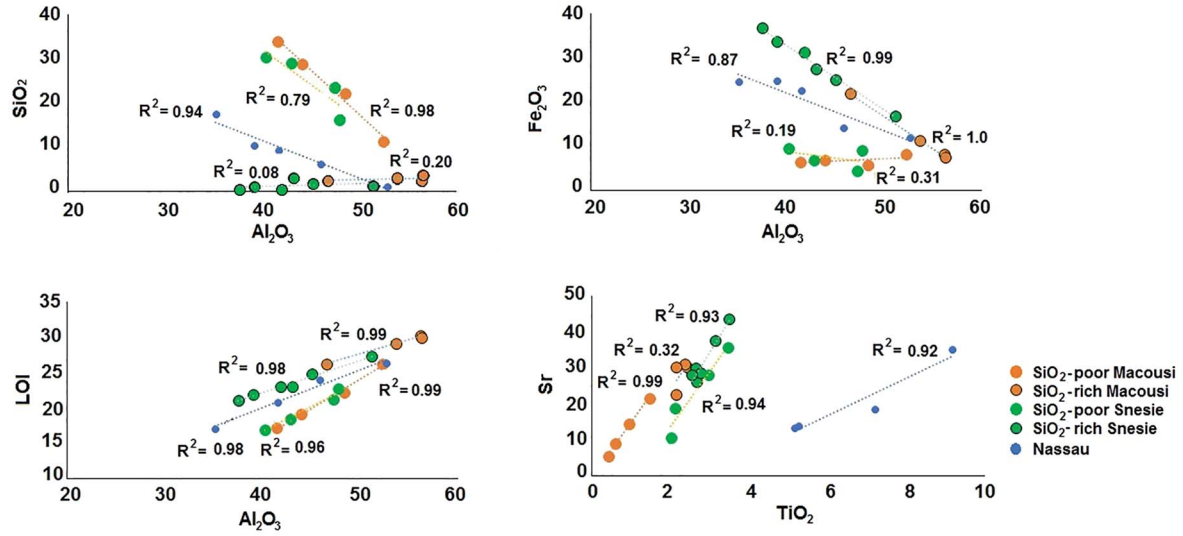

Fig. 11. The SiO_2-Al_2O_3, Al_2O_3-Fe_2O_3, LOI- Al_2O_3 and Sr-TiO_2 plots for analyzed bauxite profiles. Note the differences in inter-element relationships between SiO_2-poor (top) and SiO_2-rich (bottom) parts of the profiles.

for pisolith formation (Boulangé, 1984; Trolard and Tardy, 1987).

5.2. Geochemical effects of weathering

The petrographic observations and chemical compositions indicate that aluminium is mostly present as gibbsite, with minor amounts in kaolinite, boehmite, and Al-bearing goethite and hematite. Iron is mainly hosted in goethite and hematite, titanium in anatase/rutile and ilmenite, while silicon mostly resides in kaolinite, and occasionally in minor amounts of residual quartz, feldspar and other silicates from the original parent rocks. Chemical indicators confirm that the investigated bauxite deposits represent advanced stages of weathering. Values for the Chemical Index of Alteration [CIA = $100xAl_2O_3 / (Al_2O_3 + CaO + Na_2O + K_2O)$; Nesbitt and Young, 1982; Wei et al., 2014] are > 99 for all samples from the Snesie, Macousi and Nassau profiles, consistent with efficient removal of Ca, Na and K. According to the Al_2O_3-Fe_2O_3-SiO_2 classification of Schellmann (1986), the degree of lateritization ranges between moderate in the bottom parts to strong in the top parts of the bauxite profiles (Fig. 9). The diagrams of Fig. 9 further reveal that each area has its own Al_2O_3-Fe_2O_3-SiO_2 signature, apparently reflecting differences in parent-rock controls and/or weathering histories.

The effect of weathering can also be inferred from normalized major and trace element patterns. In absence of data for pristine parent rocks and in view of the chemical variability of metamorphic rocks in the Bakhuis area (Klaver et al., 2015), the concentrations were normalized against upper continental crust (Rudnick and Gao, 2004) in order to illustrate first-order chemical weathering effects (Fig. 10). The patterns show a consistent depletion of fluid-mobile elements (Si, Mn, Na, K, Sr, Ba) and a relative enrichment of "immobile" elements (Al, Ti, Sc, V, Cr, As, Zr, Nb, Hf, Ta, Th). SiO_2-poor (< 5 wt%) samples in the top parts of the profiles tend to be relatively enriched in most elements, with the exception of the highly mobile 1^+ and 2^+ charged ones (Figs. 7, 8, 10). A comparison of the patterns for the parent rock (BAK-02) and altered equivalent (BAK-02) from Bakhuis Base Camp demonstrates the relative enrichment of Al, Ti, Fe, V, Zr, Nb, Hf, Ta, Pb, Th, U in the weathering residue.

5.2.1. Mobilization and redistribution of major elements

Inter-element relationships show clear differences between SiO_2-poor (< 5 wt%) upper parts and SiO_2-richer (> 5 wt%) lower parts of the Snesie and Macousi profiles, which points to differences in weathering regime and mineralogical control. In both cases Al_2O_3 correlates positively with LOI, albeit along different trends (Fig. 11). For the SiO_2-richer intervals, where Al_2O_3 correlates negatively with SiO_2, the Al_2O_3-LOI (and Al_2O_3-SiO_2) trends are largely determined by the proportions of gibbsite and kaolinite. In these intervals, Al_2O_3 correlates relatively strongly with almost all other elements with a 3^+, 4^+, or 5^+ valence, except for Fe. These systematics are consistent with residual enrichment of relatively immobile elements following the breakdown of silicate minerals and removal of Si and associated soluble components.

In contrast, in the SiO_2-poor parts where Al_2O_3 is almost exclusively hosted in gibbsite, there is no correlation with SiO_2. Instead, there is a strong inverse relationship between Al_2O_3 and Fe_2O_3, reflecting the increasing amount of Fe-rich phases towards the top of the profiles. In the Macousi profile, where vertical concentration trends are relatively smooth and undisturbed (Fig. 11), there are also clear positive correlations (R^2 = 0.79–0.98) between Al_2O_3 and Nb, Ta, Pb, Th, REE, Sr, Ba, and negative correlations (R^2 = 0.84–0.99) with Sc, V, Cr, Zn, As, a group of elements that tend to be associated with Fe. In the top parts of Snesie and Macousi profiles, Fe_2O_3 correlates positively with P_2O_5 (R^2 = 0.74 and 1.0, respectively), and with Sc, V, Cr and As (all R^2 > 0.97) only at Macousi. In the bottom parts, correlations with Fe_2O_3 are poor, except for Sc (R^2 = 94) and V (R^2 = 99) at Snesie.

The most conspicuous feature in the Nassau profile is that TiO_2 strongly correlates with many trace elements (e.g., R^2 > 0.9 for Zn, Sr, Y, Zr, Nb, Ce, Yb, Hf, Ta), which is comparable to systematics in the SiO_2-richer part of the Macousi profile that can be largely attributed to residual enrichment effects.

5.2.2. Mobilization and redistribution of rare earth elements

Numerous studies of other lateritic covers of metamorphic and igneous rocks in humid tropical regions have demonstrated the mobility of REE during weathering and differences in the behavior of LREE and HREE. Often, upper Fe-rich layers in lateritic weathering profiles are depleted in REE, whereas accumulation occurred in deeper layers such as the basal saprolite rock (Braun et al., 1993, 1998; Kamgang Kabeyene Beyala et al., 2009; Sanematsu et al., 2013; Berger and Frei, 2014). In other cases, net mass gains in REE have been observed in

uppermost bauxite levels relative to underlying layers (e.g., Boulangé and Colin, 1994). Frequently, vertical variations point to differences in behavior among the REE, such as preferential leaching and removal of HREE or LREE from the supergene zone, the development of Ce anomalies, or preferential fixation through adsorption or incorporation in secondary minerals.

The UCC-normalized REE concentrations in the Snesie, Macousi and Nassau profiles show different patterns (Fig. 10). In the Snesie deposits, the LREE are enriched relative to the HREE, whereas the Macousi trends show little fractionation and the Nassau profile a flat pattern for the LREE and a gradual enrichment towards the HREE. Overall, the REE seem to be residually enriched in the SiO_2-poor ferruginous top parts of the sequences (Fig. 10) relative to strongly leached elements (although this does not necessarily exclude their mobility), and there is considerable vertical variability in detail, in particular in the Snesie profile. There is no evidence for a significant Ce anomaly in any of the settings.

The REE trends show little variation within each individual bauxite deposit. This might be the result of insignificant fractionation among the REE in the weathering history, so that the different pattern shapes largely reflect variations of the parent rocks. Alternatively, redistribution of the REE was accompanied by substantial fractionation but the effects from mobility differences during incipient leaching have been obliterated due to the advanced stage of weathering that the current sequences have reached. In absence of samples from pristine parent rocks, the extent to which weathering has re-shaped the REE patterns is difficult to test for Snesie, Macousi and Nassau but some insight into REE mobility and fractionation can be obtained by comparing the patterns of the amphibolite parent rock (BAK-02) and its strongly weathered equivalent (BAK-01) from Bakhuis Base Camp (Fig. 10). The differences in UCC-normalized distributions suggest that REE were mobile during weathering resulting in lower overall concentrations BAK-01. Also, trends are not parallel, and MREE tend to be preferentially depleted. Finally, the positive Eu anomaly seen in the proposed parent rock is virtually absent in the weathered rock, apparently due to a stronger removal of Eu^{2+} upon breakdown of plagioclase and other primary minerals.

Because the REE pattern for BAK-01 is comparable in shape to that of the Nassau samples, similar REE mobility and preferential loss of MREE may also have affected the bauxite in this area. Topp et al. (1984) also inferred differences in behavior of light and intermediate REE from enrichments at different levels in a 12.5 m laterite profile on Proterozoic charnockitic rocks in the same region as the Bakhuis profiles studied here. They reported an enrichment of Sm and Eu in a clay-rich zone near the base, presumably due to accumulation of species leached out higher up in the profile.

5.2.3. Possible mineral controls of trace-element distributions

Multiple studies have provided evidence for mineralogical controls of trace-element behavior during lateritic weathering, either through the presence of particular (accessory) host minerals in the parent rock, their stability in the course of alteration, uptake by secondary minerals or sorption onto surfaces (Nesbitt, 1979; Banfield and Eggleton, 1989; Braun et al., 1993, 1998). Primary accessory phases that typically host REE and many other high-valence elements in parent rocks of lateritic bauxite include zircon, phosphates (monazite, apatite, xenotime), Ti-bearing minerals (rutile/anatase, titanite, ilmenite) and allanite. Phosphate weathering will usually release a significant amount of the REE budget, which may then become fixed in secondary phosphates such as rhabdophane and florencite, unless advanced weathering ultimately leads to their breakdown as well (Laveuf and Colin, 2009). The observed trace-element distributions may thus be partly caused by the nature and quantity of original host minerals, differences in their resistance against weathering and/or different behavior after element release (e.g. storage in newly formed minerals or adsorption onto mineral surfaces).

Of the most relevant primary accessory minerals, zircon is a ubiquitous phase in many samples of the profiles studied, whereas monazite, apatite, anatase/rutile were occasionally detected especially in the Bakhuis Base Camp samples. Secondary phosphates were not identified in any of the samples but their presence can certainly not be excluded. Because REE and actinide-bearing accessory minerals in Precambrian high-grade gneissic terrains commonly include monazite, apatite, zircon, titanite, allanite and xenotime (Harlov, 2011), it is reasonable to suppose that all of these phases potentially played a role in element re-distribution during bauxitization of the Bakhuis deposits, given the high-grade character (up to granulite facies) of parent rocks in this area. Inspected samples of the meta-volcanic parent rocks in the Nassau area contain zircon, anatase/rutile, while titanite may be present as well.

The often excellent correlation between TiO_2 and Sr (Fig. 11) in the studied areas is remarkable, given the expected mobile behavior of the latter, and suggests that a significant part of the Sr budget is stored in titanite, as this mineral is also capable of accommodating many of the high-valence elements (Tiepolo et al., 2002). If this is the case, then the inferred MREE depletion at Bakhuis Base Camp and Nassau profiles could reflect breakdown of titanite, as this is generally enriched in the MREE (Green and Pearson, 1986; Tiepolo et al., 2002). The LREE enrichment in the Snesie profile (Fig. 10) could be due to monazite, apatite, or their breakdown products, as these phosphates preferentially incorporate LREE (Boulangé et al., 1990; Horbe and Da Costa, 1999; Laveuf and Colin, 2009; Babechuk et al., 2015).

From the above considerations we infer that weathering effects on mobility and redistribution of REE and other trace elements were significant in all of the area studied, and affected even the least mobile elements. Difference in element distribution patterns between the individual profiles likely reflect a combination of primary compositional differences of parent rocks, the nature and content of accessory phases and their unequal behavior during weathering.

5.3. Parent rocks and their influences

Our results provide new insights into the diversity of crystalline parent rocks of the Surinamese highland bauxites and their influence on properties of the ultimate weathering products. The variability of the original high-grade metamorphic rocks in the Bakhuis Mountains is apparent in the differences between the Bakhuis Base Camp bauxite that formed at the cost of pyroxene amphibolite and the weathering profiles of Snesie and Macousi where pristine parent rocks were not recovered. The higher Al_2O_3/Fe_2O_3 ratios and less complex vertical variability in chemistry in the Macousi profiles relative to the Snesie profiles (Figs. 7 and 11), as well as differences in trace-element patterns (Fig. 10), reflect distinct properties of the parent rocks. The compositional banding and altered relic blasts in Snesie saprolite samples point to a sillimanite-bearing gneissic parent rock. The LREE enrichment is consistent with a metasedimentary source, assuming that the apparent REE mobility did not seriously modify the original tendency of the pattern. The parent rock of the Macousi profiles was probably different in view of the chemistry but the petrography is inconclusive. The higher Al_2O_3/Fe_2O_3 ratios may be indicative of a more felsic parent than that of the Snesie profiles.

The Macousi parent rock may have been similar to the pyroxene amphibolitic parent rock at Bakhuis Base Camp on an adjacent plateau (Area 10.1), considering the similar shapes of the trace-element patterns of the weathered rocks (Fig.10). In turn, the pattern of the unweathered pyroxene amphibolite (BAK-02) is grossly similar to that of fresh granulites of the Bakhuis Mountains (Klaver et al., 2015), which suggests that Macousi and Bakhuis Base Camp parents form part of the granulite suite, as is also consistent with the depletion in Th and U.

The chemical and petrographic data also indicate that the bauxite occurrences in eastern Suriname originated on various parent rocks, in agreement with the variability of rock types such as greenschist-facies metabasalts and other meta-igneous rocks that make up the Paramaka

Formation (Aleva, 1994; Kroonenberg et al., 2016). Average Al_2O_3/Fe_2O_3 ratios are highest at Nassau and lowest at Lely, suggesting that the bauxite formed on igneous parent rocks with different degrees of differentiation. The parent rock of Nassau Plateau C is probably a meta-andesite or meta-basalt, based on the relict texture of a piece of saprock-saprolite. A fresh rock from Brownsberg with actinolite, clinozoisite and chlorite is consistent with a relatively mafic extrusive rock, metamorphosed in greenschist facies.

The variation in parent rock composition and texture, together with differences in drainage and climate conditions, age and tectonic stability of surfaces have affected the extent of lateritization, the resulting weathering mineralogy and thicknesses of bauxite bodies in the study areas. Original stratigraphic heterogeneity will have added to the diversity and may explain the local presence of lenses of kaolinite-rich material within the bauxite horizon, and lenses of bauxite material within the kaolinitic saprolite (Doeve, 1955; Coutinho, 1967; Janssen, 1979; Aleva and Hilversum, 1984). The diversity in rock types and weathering conditions explains the general lens-shaped morphology of the plateau-type bauxite bodies, the absence of bauxite in certain areas of the Bakhuis and Nassau Mountains, and local exposures of fresh bedrock and boulders within the main bauxite body of Bakhuis (Coutinho, 1967).

6. Summary and conclusions

Textural, mineralogical and geochemical information on lateritic plateau bauxites of Suriname has been investigated to assess the influence of bedrock lithology on the compositional properties of weathering profiles developed on a variety of Proterozoic crystalline basement rocks of the Guiana Shield. Studied bauxite deposits of the Bakhuis Mountains, Nassau Mountains, Lely Mountains and Brownsberg are distributed at relatively high topographic elevations in the country's interior as relics of a succession of stepped planation surfaces with a regional extent, which formed as a result of long-term tectonic stability and periodic continental uplift. The parent rocks range from (ultra)high-temperature metamorphic gneissic and amphibolitic rocks in the Bakhuis Mountains (granulite belt in west Suriname) to greenschist-facies metabasalts and other meta-igneous rocks in the other areas (Greenstone belt in east Suriname).

All of the investigated profiles show a strong mineralogical and chemical zoning according to the degree of lateritization, which ranges between moderate in the bottom parts to strong in the top layers. The bauxites contain gibbsite as principal Al-hosting mineral, have a ferruginous surface and grade downward into kaolinite-rich saprolite and altered bedrock. Different signatures of the parent rocks of the deposits are expressed by variable Al_2O_3/Fe_2O_3 ratios and TiO_2 concentrations being markedly higher in the bauxites formed on top of metavolcanics of the greenstone belt than in those covering the granulite belt. The Nassau deposit stands out by an abundance of pisoliths consisting of hematite, goethite and gibbsite, which supposedly reflect fluctuating hydration, drainage and redox conditions. The presence of minor amounts of boehmite further supports a hydration control.

First-order effects of chemical weathering are a consistent depletion of fluid-mobile elements (Si, Mn, Na, K, Sr, Ba) and a relative enrichment of “immobile” elements (Al, Ti, Sc, V, Cr, As, Zr, Nb, Hf, Ta, Th). The SiO_2-poor top parts of the profiles tend to be most enriched in the latter group. Normalized element abundances are distinct for different areas but show uniform patterns in individual profiles. Frequent absence of pristine bedrock equivalents precludes quantitative assessments of mass changes.

Despite this internal homogeneity of chemical patterns, weathering processes have induced significant deviations from original signatures and generated fractionation among REE and other “immobile” trace-elements. Differences in element distribution patterns between the individual profiles likely reflect a combination of primary compositional differences of parent rocks, the nature and content of accessory phases and their unequal behavior during weathering. Field appearances, textural relationships between secondary minerals and locally complex chemical profiles signal a polygenetic character of the bauxites, which is inferred to be associated with multiple cycles of weathering since Late Cretaceous times.

Acknowledgements

The authors would like to thank Tilly Bouten, Helen de Waard and Anita van Leeuwen-Tolboom for help with analytical work at Utrecht University, and Pieter Vroon for XRF data produced with the facility at the Free University of Amsterdam. The Bauxite Institute of Suriname and Suralco kindly provided major-element data and samples from exploration drilling campaigns. This research was funded by a grant from the Suriname Environmental and Mining Foundation (SEMIF) (SEMIF 014-11).

Appendix A

Comparison of trace-element contents obtained for the BX-N bauxite standard by LA-ICPMS on lithium borate glass beads with compilation values (Govindaraju, 1995).

	Compilation	Measured	Reliability		Compilation	Measured	Reliability
	Value	Value	(Diff. %)		Value	Value	(Diff. %)
As	115	131	14	Pr	54	51	− 5.2
Ba	30	33	11	Rb	3.6	2.9	− 19
Ce	520	558	7.4	Sc	60	72	20
Cr	280	346	24	Sm	22	21	− 4.5
Dy	18.5	18.6	0.7	Sr	110	109	− 1.3
Er	11	11	0.2	Ta	4.6	3.7	− 18
Eu	4.4	4.0	− 9.5	Tb	3	2.7	− 11
Gd	20	17	− 13	Th	50	46	− 7.2
Hf	15.2	13.9	− 8.8	U	8.8	7.8	− 11
Ho	4.1	3.7	− 10	V	350	435	24
La	355	n.d.	n.d.	Y	114	118	3.4
Lu	1.8	1.7	− 7.2	Yb	11.6	11.9	2.7
Nb	52	55	4.9	Zn	80	82	2.2
Nd	163	156	− 4.2	Zr	550	564	2.5
Pb	135	129	− 4.2				

Appendix B

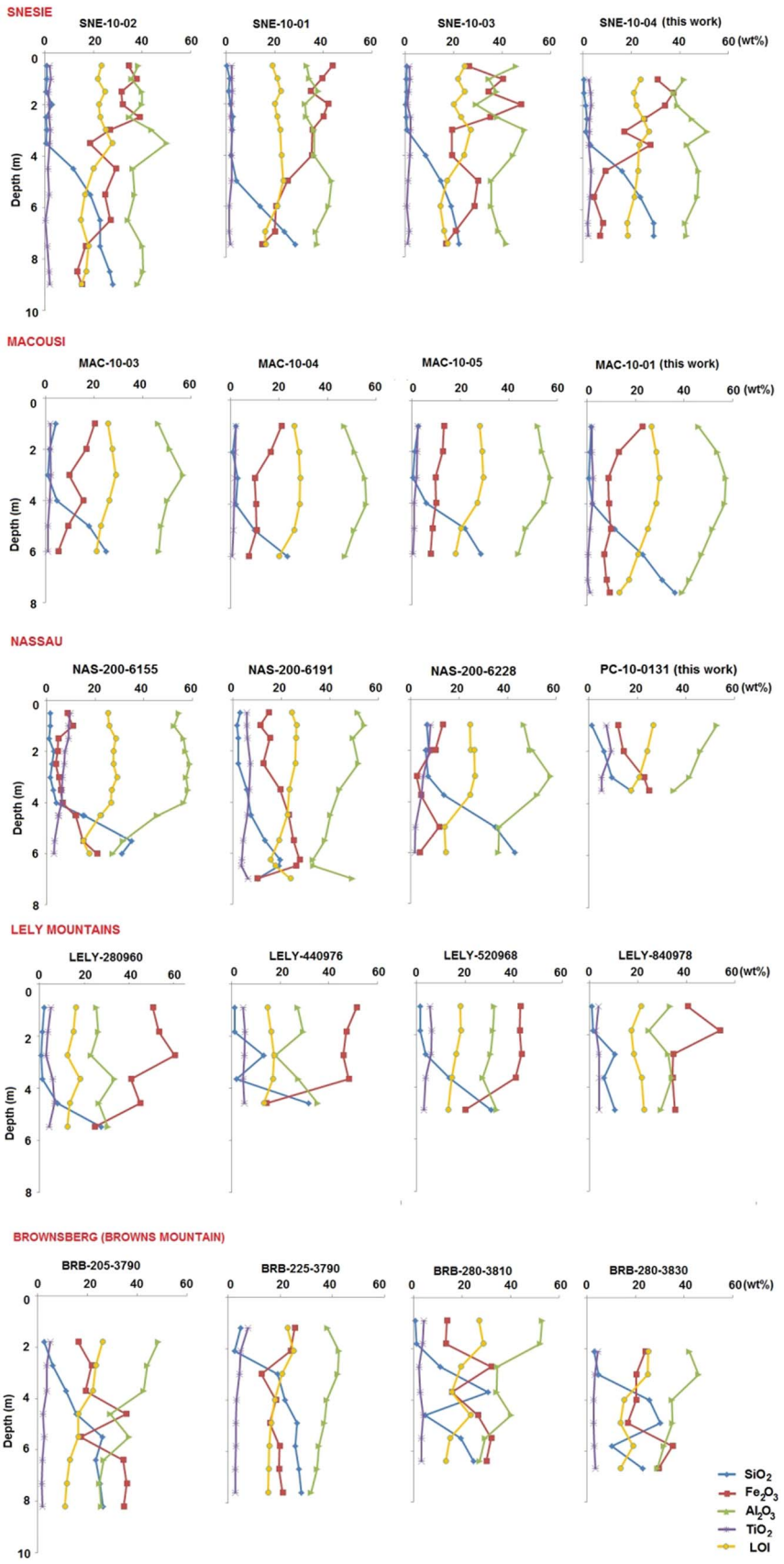

Vertical variations of major-element contents in weathering profiles from the Bakhuis area (Snesie and Macousi), Nassau Mountains, Lely Mountains and Brownsberg.

References

Aleva, G., 1965. The buried bauxite deposits of Onverdacht, Surinam, South America. Geol. Mijnb. 44, 45–58.

Aleva, G., 1979. Bauxitic and other duricrusts in Surinam. A review. Geol. Mijnb. 58, 321–336.

Aleva, G., 1984. Lateritization, bauxitization and cyclic landscape development in the Guiana Shield. In: Jacob Jr.L. (Ed.), Bauxite [Bauxite Symposium, Los Angeles, California, 1984, Proceedings]. American Institute of Mining, Metallurgical, and Petroleum Engineers, New York, pp. 297–318.

Aleva, G.J.J., 1994. Laterites. In: Concepts, Geology, Morphology and Chemistry. Wageningen, ISRIC.

Aleva, G., Hilversum, A., 1984. West Suriname: known deposits and potential. In: Jacob Jr.L. (Ed.), Bauxite: Proceedings of 1984 Bauxite Symposium, Los Angeles. American Institute of Mining Metallurgical and Petroleum Engineers, New York, pp. 319–348.

Aleva, G., Wong, Th., 1998. The history of bauxite exploration and mining in Suriname. In: The History of Earth Sciences in Suriname. Royal Netherlands Academy of Arts and Sciences, and Netherlands Institute of Applied Geoscience. TNO, pp. 275–310.

Babechuk, M., Widdowson, M., Murphy, M., Kamber, B., 2015. A combined Y/Ho, high field strength element (HFSE) and Nd isotope perspective on basalt weathering, Deccan traps, India. Chem. Geol. 369, 25–41.

Banfield, J., Eggleton, R., 1989. Apatite replacement and rare earth mobilization, fractionation, and fixation during weathering. Clay Clay Miner. 37 (2), 113–127.

Bánki, O., Ter Steege, H., Jansen-Jacobs, M., Raghoenandan, U., 2008. Plant Diversity of the Nassau Mountains, Suriname; Report of the 2003 Expedition. Internal Report. NHN-Utrecht, BBS-Paramaribo, Utrecht, Netherlands. Paramaribo, Suriname, pp. 1–52.

Bárdossy, G., Aleva, G., 1990. Lateritic bauxites. In: Developments in Economic Geology. 27 Elsevier Science Publishing.

Bauxite Institute Suriname, 2009. Suriname as a source of bauxite and alumina. In: Prospects for Growth? 15th Bauxite and Alumina Seminar, February 2009, Montega Bay, Jamaica.

Berger, A., Frei, R., 2014. The Fate of Chromium During Tropical Weathering; A laterite profile from Central Madagascar. 213. pp. 512–532.

Billiton, 1979. Unpublished Results. Feasibility Study of the Bakhuis Mountains, Internal Report. pp. 1–8.

Bogatyrev, B., Zhukov, V., Tsekhovsky, G., 2009. Formation conditions and regularities of the distribution of large and superlarge deposits. Lithol. Miner. Resour. 44 (2), 135–151.

Bosma, W., Kroonenberg, S.B., Van Lissa, R.V., Maas, K., De Roever, E.W.F., 1984. An explanation to the geology of Suriname. In: Contributions to the Geology of Suriname. Geologisch Mijnbouwkundige Dienst Suriname, Paramaribo, pp. 1–8.

Boulangé, B., 1984. Les formations bauxitiques latéritiques de Côte d'Ivoire. 1055 Travaux et documents d'ORSTOM, Paris. 175.

Boulangé, B., Colin, F., 1994. Rare earth element mobility during conversion of nepheline syenite into lateritic bauxite at Passa Quatro, Minais Gerais, Brazil. Appl. Geochem. 9, 701–711.

Boulangé, B., Muller, J., Sigolo, J., 1990. Behaviour of the Rare Earth Elements in a Lateritic Bauxite From Syenite (Brazil). In: Geochemistry of the Earth's Surface and of Mineral Formation. Second International Symposium, July 1990, Aix en Provence, France, pp. 350–351.

Braun, J., Pagel, M., Herbilln, A., Rosin, C., 1993. Mobilization and redistribution of REEs and thorium in a syenitic lateritic profile: A mass balance study. Geochim. Cosmochim. Acta 57 (18), 4419–4434.

Braun, J., Viers, J., Dupre, B., Polve, M., Ndam, J., Muller, J., 1998. Solid/liquid REE fractionation in the lateritic system of Goyoum, East Cameroon: The implications for the present dynamics of the soil covers of the humid tropical regions. Geochim. Cosmochim. Acta 62 (2), 273–299.

Coutinho, H., 1967. Unpublished Results. Suralco Final Report Area 10.1, Suralco Internal Report, Paramaribo. pp. 4–6.

De Roever, E., Kieft, C., Murray, E., Klein, E., Drucker, W., 1976. Surinamite, a new Mg-Al silicate from the Bakhuis Mountains, western Surinam: I. Description, occurrence and conditions of formation. Am. Mineral. 61, 193–199.

De Roever, E., Lafon, J., Delor, C., Cocherie, A., Rossi, P., Guerrot, C., Potrel, A., 2003. The Bakhuis ultrahigh- temperature granulite belt (Suriname); 1. Petrological and geochronological evidence for a counterclock wise P-T path at 2.07-2.05 GA. Géol. Fr. 175–205 (2-3-4).

De Vletter, D.R., 1984. Economic geology and mineral potential of Suriname. In: De Vletter, D.R. (Ed.), Geology of Suriname 8. 27. Mededelingen Geologisch Mijnbouwkundige Dienst, Suriname, pp. 91–129.

De Vletter, D.R., Aleva, G., Kroonenberg, S., 1998. Research into the Precambirian of Suriname. In: The History of Earth Sciences in Suriname. Royal Netherlands Academy of Science, Netherlands Institute of Applied Geoscience TNO, Amsterdam, pp. 15–63.

Delor, C., de Roever, E., Lafon, J., Lahondere, D., Rossi, P., Cocherie, A., Guerrot, C., Potrel, A., 2003. The Bakhuis ultrahigh-temperature granulite belt (Suriname): II. Implication for late Transamazonian crustal stretching in a revised Guiana Shield framework. Geology of France and surrounding area. (France No 2-3-4) pp. 207–231.

Delvigne, J., 1998. Atlas of Micromorphology of Mineral Alteration and Weathering. Mineral Association of Canada.

Doeve, G., 1955. De bauxiet exploratie op het Nassau gebergte (in Dutch). Unpublished report Geologisch Mijnbouwkundige Dienst Suriname, Paramaribo, pp. 1–68.

Dos Muchangos, A.C., 2000. Mineralogy and Geochemistry of Bauxite and Bentonite Deposits from Mozambique. Dissertation at University of Utrecht, Faculty of Earth Sciences.

Eggleton, R.A., Taylor, G., 2008. Impact of fire on the Weipa Bauxite, Northern Australia. Aust. J. Earth Sci. 55 (1), 83–86.

Feret, F., Authier-Martin, M., Sajó, I., 1997. Quantitative phase analysis of Bidi Koum Bauxites (Guinea). Clay Clay Miner. 45 (3), 418–427.

Fitzpatrick, R., Schwertmann, U., 1982. Al-substituted goethite—an indicator of pedogenic and other weathering environments in South Africa. Geoderma 27, 335–347.

Gong, X., Nie, Z., Qian, M., Lui, J., Pederson, D., Hobbs, D., McDuffie, N., 2002. Gibbsite to Boehmite Transformation in Strongly Caustic and Nitrate Environments. (Document nr. WSRC-MS-2002-00850) US Department of Energypp. 1–3.

Govindaraju, K., 1995. Working values with confidence limits for twenty-six CRPG, ANRT and IWG-GIT geostandards. Geostand. Newslett. 19, 1–32.

Green, T., Pearson, N., 1986. Ti-rich accessory phase saturation in hydrous mafic-felsic composions at high P, T. Chem. Geol. 54 (3–4), 185–201.

Harlov, D., 2011. Petrological and experimental application of REE- and actinide-bearing accessory minerals to the study of Precambrian high-grade gneiss terranes. Geol. Soc. Am. Mem. 207, 13–24.

Helgeson, H., 1971. Kinetics of mass transfer among silicates and aqueous solutions. Geochim. Cosmochim. Acta 35, 421–469.

Horbe, A., Anand, R., 2011. Bauxite on igneous rocks from Amazonia and western of Australia: Implication for weathering process. J. Geochem. Explor. 111 (1–2), 1–12.

Horbe, A., Da Costa, M., 1999. Geochemical evolution of a lateritic Sn-Zr-Th-Nb-Y-Ree-bearing ore body derived from apogranite: the case of Pitinga, Amazonas-Brazil. J. Geochem. Explor. 66, 339–351.

Janssen, J., 1963. Unpublished Results. Reconnaissance Exploration for Bauxite in the Adampada-Kabalebo Area 1961–1963. Internal Grassalco Report, Paramaribo. pp. 1–5.

Janssen, J., 1977. Bauxite. In: Encyclopedia of Suriname. Bruijining C.F.A. and Voorhoeve, Elsevier, Amsterdam, pp. 227–229.

Janssen, J., 1979. Unpublished Results. Bauxite and Laterite Hard Caps in Suriname. Internal Grassalco Report, Paramaribo. pp. 1–12.

Kamgang Kabeyene Beyala, V., Onana, V., Priso, E., Parisot, J., Ekodeck, G., 2009. Behaviour of REE and mass balance calculations in a lateritic profile over chlorite schists in South Cameroon. Chem. Erde 69, 61–73.

Kawano, M., Tomita, K., 1995. Experimental study on the formation of clay minerals from obsidian by interaction with acid solution at 150 °C and 200 °C. Clay Clay Miner. 43 (2), 212–222.

King, L.C., Hobday, D.K., Mellody, M., 1964. Unpublished Results. Cyclic denudation in Surinam. Geologische Mijnbouwkundige Dienst Suriname, Paramaribo, pp. 1–12.

Klaver, M., de Roever, E., Nanne, J., Mason, P., Davies, G., 2015. Charnockites and UHT metamorphism in the Bakhuis Granulite Belt, western Suriname; evidence for two separate UHT events. Precambrian Res. 262, 1–19.

Krook, L., De Roever, E., 1975. Some Aspects of Bauxite Formation in the Bakhuis Mountains, Western Suriname. Anais 10a Conferencia Geologica Interguianas, Bélem. 1. pp. 686–695.

Kroonenberg, S., 1976. Amphibolite facies and granulite facies metamorphism in the Coeroenie Lucie Area, SW Suriname. In: Mededelingen Geologisch Mijnbouwkundige Dienst Suriname, Paramaribo. 25. pp. 109–209.

Kroonenberg, S., De Roever, E., 1975. Dumortierite in cordierite pseudomorphs and in shear zones in high grade metamorphic rocks from western Suriname. In: Mededelingen Geologisch Mijnbouwkundige Dienst Suriname, Paramaribo. 23. pp. 255–259.

Kroonenberg, S., Melitz, P., 1983. In: Van den Berg, M., Felix, R. (Eds.), Summit Levels, Bedrock Control and the Etchplain Concept in the Basement of Suriname. 62. Geologie en Mijnbouw, pp. 389–399 (Special issue in the honor of J. De Jong).

Kroonenberg, S., De Roever, E., Fraga, L., Reis, N., Faraco, M., Lafon, J., Cordani, U., Wong, Th., 2016. Paleoproterozoic evolution of the Guiana Shield in Suriname: A revised model. Neth. J. Geosci., Geol. Mijnb. 95 (4), 491–522.

Laveuf, C., Colin, F., 2009. A review on the potentiality of Rare Earth Elements to trace pedogenetic processes. Geoderma 154 (1-2), 1–12.

Meyer, M., Happel, U., Hausberg, J., Wiechowski, A., 2002. Geometry and anatomy of the Los Pijiguaos bauxite deposit, Venezuela. Ore Geol. Rev. 20 (1–2), 27–54.

Monsels, D.A., 2016. Bauxite deposits in Suriname: Geological context and resource development. Neth. J. Geosci., Geol. Mijnb. 95 (4), 405–418.

Mutakyahwa, M., Valeton, I., 1995. Late Cretaceous - Lower Tertiary Weathering Event and Its Laterite-Bauxite Formation in Tanzania. 78. Mitteilungen aus dem Geologisch - Paläontologischen Institut der Universität Hamburgpp. 1–66.

Nahon, D., Merino, E., 1997. Pseudomorphic replacement in tropical weathering: Evidence, geochemical consequences and kinetic-rheological origin. Am. J. Sci. 29, 393–417.

Nesbitt, H., 1979. Mobility and fractionation of rare earth elements during weathering of granodiorite. Nature 279, 206–210.

Nesbitt, H., Young, G., 1982. Early Proterozoic climates and plate motions inferred from major element chemistry of lutites. Nature 299, 715–717.

Ouboter, P., Jairam, R., Wan Tong You, K., 2007. Additional records of amphibians from the Nassau Mountains, Suriname. In: Alonso, L., Mol, J. (Eds.), A rapid Biological assessment of the Lely and Nassau Plateaus, Suriname (with additional information on the Brownsberg Plateau). RAP bulletin of Biological Assessment 43 Conservation International, Arlington, USA, pp. 128–129.

Patterson, S., Kurtz, H., Olson, J., Neeley, C., 1986. World Bauxite Resources; Geology and Resources of Aluminum. U.S. Geological Survey professional paper, 1076-B. United States Government Printing Office, Washington.

Pollack, H., 1981. Bauxites and laterites of the Bakhuis Mountain Zone, western Suriname; a general description with emphasis on geomorphology and chemistry. In: Lateritization processes, Proceedings of International seminar on lateritization processes, December 1979. Oxford and IBH Publushing Company, New Dehli (270-268).

Pollack, H., 1983. Land surfaces and lateritization in Suriname. In: Melfi, A.J., Carvalho, A. (Eds.), Proceedings of International Seminar on Lateritization Processes, 1982, São

Paulo, Brazil, pp. 295–308.
Priem, H., Boelrijk, N., Hebeda, E., Verdurmen, E., Verschure, R., 1971. Isotopic ages of the Trans-Amazonian acidic magmatism and the Nickerie metamorphic episode in the Precambrian basement of Suriname, South America. GSA Bull. 82 (6), 1667–1680.
Priem, H., De Roever, E., Bosma, W., 1980. A note on the age of the Paramaka metavolcanics in northern Suriname. Geol. Mijnb. 59, 171–173.
Rudnick, R., Gao, S., 2004. Composition of the continental crust. In: Holland, H., Turekian, K. (Eds.), Treatise on Geochemistry. 3. Elsevier, Amsterdam, pp. 1–64.
Saalfeld, H., 1958. The dehydration of gibbsite and the structure of a tetragonal γ-Al_2O_3. Clay minerals. Mineral. Soc. 3 (19), 249–257.
Sanematsu, K., Kon, Y., Imai, A., 2013. Geochemical and mineralogical characteristics of ion-adsoprtioon type REE mineralization in Phuket, Thailand. Mineral. Deposita 48 (4), 437–451.
Schellmann, W., 1983. A New Definition of Laterite. 18. Natural Resources and Development, Hannover/Tubingen, pp. 7–12.
Schellmann, W., 1986. A new definition of laterite. On the Geochemistry of laterites. Chem. Erde 45, 39–43.
Schellmann, W., 1994. Geochemical differentiation in laterite and bauxite formation. Catena 21, 131–143.
Scott, K., Pain, C., 2009. Regolith Science. Csiro publishing, Australia and Springer, The Netherlands.
SPS and OAS (Stichting Planbureau Suriname and Organization of American States), 1988. Suriname Planatlas (in Dutch). SPS/OAS, Washington D.C.
Tardy, Y., 1997. Petrology of Laterites and Tropical Soils. Balkema, Rotterdam/Brookfield.
Tardy, Y., Nahon, H., 1985. Geochemistry of laterites, stability of Al-goethite, Al-hematite, and Fe3 + -kaolinite in bauxites and ferricretes: an approach to the mechanism of concretion formation. Am. J. Sci. 285, 865–903.
Tardy, Y., Roquin, C., 1998. Dérive des continents, paléoclimats et alterations tropicales. BRGM (473 pp).
Taylor, G., Eggleton, R., 2008. Genesis of pisoliths and of the Weipa Bauxite deposit, northern Australia. Aust. J. Earth Sci. 55, 87–103.
Ter Steege, H., Bánki, O., Haripersaud, P., 2006. Plant diversity of the bauxite plateaus of North east Suriname. In: Alonso, L., Mol, H. (Eds.), A Rapid Biological Assessment of the Lely and Nassau Plateaus, Suriname (With Additional Information on the Brownsberg Plateau) RAP Bulletin, pp. 76–85.
Théveniaut, H., Freyssinet, Ph., 2002. Timing of lateritization on the Guiana Shield: synthesis of paleomagnetic results from French Guiana and Suriname. In: Palaeography, Palaeoclimatology, Palaeoecology. 178. Elsevier, pp. 91–117.
Tiepolo, M., Oberti, R., Vannucci, R., 2002. Trace-element incorporation in titanite: constrains from experimentally determined solid/liquid partition coefficients. Chem. Geol. 1, 105–119.
Topp, S.E., Salbu, B., Roaldset, E., Jørgensen, P., 1984. Vertical distribution of trace elements in laterite soil (Suriname). Chem. Geol. 47, 159–174.
Trolard, F., Tardy, Y., 1987. The stabilities of gibbsite, boehmite, alumious goethite and aluminous hematite in bauxites, ferricretes and laterites as a function of water activity, temperature and particle size. Geochim. Cosmochim. Acta 51, 945–957.
Valeton, I., 1972. Bauxites. Elsevier, Amsterdam.
Valeton, I., 1983. Palaeoenvironment of lateritic bauxites with vertical and lateral differentiation. Geol. Soc. Lond., Spec. Publ. 11 (1), 77–90.
Van den Bergh, J., 2011. Executive Summary for the Nassau Plateau Bauxite Project. Internal Suralco Report. pp. 1–14.
Van der Hammen, T., Wijmstra, T., 1964. A palynological study on the Tertiary and the Upper Cretaceous of British Guiana. Leidse. Geol. Meded. 30, 183–241.
Van Kersen, J., 1956. Bauxite deposits in Suriname and Demerara (British Guiana). (Thesis Leiden; also published in) 21. Leidse Geologische Mededelingenpp. 247–375.
Van Lissa, R., 1975. Review of bauxite exploration in the coastal pain of Suriname. In: Contributions to the Geology of Suriname 4. 23. Mededelingen Geologisch Mijnbouwkundige Dienst Suriname, Paramaribo, pp. 250–254.
Velde, B., Meunier, A., 2008. Origin of Clay Minerals in Soils. Springer-Verlag, Berlin Heidelberg.
Wei, X., Ji, H., Wang, S., Chu, H., Song, C., 2014. The formation of representative lateritic weathering covers in south–central Guangxi (Southern China). Catena 118, 55–72.
Wong, Th., Krook, L., Zonneveld, J., 1998. Investigations in the coastal plain and offshore area of Suriname. In: Wong, Th., de Vletter, D., Krook, L., Zonneveld, I., van Loon, A. (Eds.), The History of Earth Sciences in Suriname. Royal Netherlands Academy of Arts and Sciences, Netherlands Institute of Applied Geoscience (TNO), pp. 73–100.
Zhu, C., Veblen, D., Blum, A., Chipera, S., 2006. Naturally weathered feldspar surfaces in the Navajo Sandstone aquifer Black Mesa, Arizona; Electron Microscopic characterization. Geochim. Cosmochim. Acta 70, 4600–4616.
Zhu, B., Fang, B., Li, X., 2010. Dehydration reactions and kinetic parameters of gibbsite. Ceram. Int. 36, 2493–2498.